

A Proposal To Construct
-SELEX-
Segmented Large-x Baryon Spectrometer

R. Edelstein, D. Gibaut, R. Lipton, D. Potter, J. Russ
Carnegie-Mellon University
Pittsburgh, PA 15213

J. Lach, L. Stutte
Fermilab
Batavia, Illinois 60510

Li Yunshan, Tang Fukun, Lang Fengfei, Li Chengze
Institute of High Energy Physics
Beijing, PRC

A. S. Denisov, V. Golovtsov, V. Grachev, A. Krivshich, N. Kuropatkin, V.
Schegelsky, N. Smirnov, N. Terentyev, L. Uvarov, A. Vorobyov,
Leningrad Nuclear Physics Institute
Leningrad, USSR

E. McCliment, C. Newsom
University of Iowa
Iowa City, Iowa 52242

C. Escobar, P. Gouffon
University of São Paulo
Brazil

P. S. Cooper
Yale University
New Haven, Connecticut 06511

November 8, 1987

Spokesperson: J. Russ
(412) 268-2755
268-2740

A PROPOSAL TO CONSTRUCT

SELEX

SEGMENTED LARGE-X BARYON SPECTROMETER

Synopsis

Heavy flavor experiments currently in progress at e^+e^- colliders or in the fixed target programs at CERN and Fermilab are aimed at collecting large samples ($>10,000$ reconstructed events) of charmed events. These experiments will provide a great deal of information about charmed meson systems, but the expected yield of charmed baryons is not large - 10% or less of the sample size. The most detailed study of the charm strange baryon Ξ_c^+ comes not from a large-statistics central production experiment at high energy but rather from a 20-day run at modest beam flux in the CERN hyperon beam. This proposal exploits the advantages in triggering and particle identification of large-x production to make a systematic study of charm baryon production and decay systematics. For the dominant ($\sim 10\%$ branching ratio) modes of these baryons, we expect to collect 10^6 triggered events in each mode per running period. This will give adequate statistics to study even highly suppressed modes.

The study of meson systematics by the Mark III spectrometer at SPEAR led to a revolution in the understanding of charmed meson decay mechanisms. No present experiment will supply a similar data set for the charmed baryons. A fixed target experiment cannot supply the absolute branching ratios that e^+e^- annihilation on the $\Psi(3770)$ resonance provides for the Mark III data. We can supply relative branching ratios for the non-leptonic and semileptonic decay

modes of charmed baryons and establish the importance of two-body resonance modes in the decay mechanism. This information, along with lifetime measurements for Λ_c^+ , Σ_c^{++} , Σ_c^+ , Σ_c^0 , Ξ_c^+ and Ω_c^0 baryons, will permit evaluation in the baryon sector of the role of color suppression, Pauli suppression, sextet enhancement and other varied mechanisms which influence decay rates of charmed hadrons. This information will be very difficult to obtain from existing spectrometers because of the wide range of particle identification methods needed to handle different decay modes. SELEX is designed specifically to do this job, as we said in the Letter of Intent.

The question of which portion of phase space is best suited to these measurements is not obvious. In the central region the cross section is the largest. There, gluon production is expected to produce baryons and antibaryons with comparable rates and characteristics. The evidence from the WA62 experiment on Ξ_c^+ production at large x and the latest analysis of ISR data on Λ_c^+ from the SFM group both indicate a forward production mechanism for charmed baryons with a general $(1-x)^2$ dependence and large, but not unreasonable, cross sections.^{1,2} The spectrum of Ξ_c^+ observed in neutron production at Fermilab from E400 was more central.³ Only new data across a broad x region will clarify the situation. We intend to construct a new apparatus with the latest capabilities in secondary vertex reconstruction, in triggering on event characteristics and in particle identification. By placing this apparatus in a hall which can provide hyperon, nucleon, and pion beams of high energy and high intensity, we are in position to make detailed studies of the production mechanisms for charmed baryons as well as the decay characteristics. While the present experiments will surely provide initial data on the general features of this physics, a second-generation experiment is both timely and necessary to make a systematic analysis.

Because the transition from central production to leading production may involve several different production processes, it is important to design an apparatus which is not limited only to large x . In this proposal the particle identification is oriented toward physics at $x > 0.25$. However, the apparatus itself has no particular cutoff at small x . The chamber sizes after the first magnet and the vertex silicon detectors are large enough to do $x=0$ physics. The acceptance curves shown in fig. 7 illustrate that SELEX triggering has useful acceptance even for $x < 0.1$ for most modes.

As we indicated in answers sent to the PAC after the letter of intent presentation, SELEX is organized to permit expansion of the range of particle identification and triggering into the central region. However, that extension is non-trivial. The group is strongly motivated to study the forward physics first, to establish the nature of leading production and to elucidate the decay mechanisms for the entire family of charmed baryons. After that initial phase, then the correlation study of $c\bar{c}$ pairs over the entire x range is of interest and additional particle tagging becomes important.

We are not held hostage to the existence of a leading baryon effect in all charmed baryon states. This is a general charm physics spectrometer with capabilities complementing the $x=0$ spectrometers now on the floor at Fermilab and CERN. For b physics this apparatus can trigger on electron p_t , and the standard trigger should yield ~ 100 events from the first run.

The hyperon beam facility in P Center has produced a series of important hyperon decay studies. If further work in this area is indicated by physics interests, the P781 apparatus is extremely well-suited to the task. The extensive software-driven triggering capabilities allow the selection of specific decay modes or kinematic regions for studying spin effects, for example. Thus, the installation of SELEX would not preclude further work of

the type that has occupied the hyperon facility up to now.

As is necessary for a second-generation device, it incorporates state-of-the-art technology in the detectors, the data acquisition and triggering architecture, and the online processing capability. However, this state-of-the-art nature exploits technologies being delivered now, not ones promised for some indeterminate future. As the discussion in the full proposal will detail, we have prototype devices now in hand or in planning for all the major detector components. Because of the collimation inherent in large-x processes, the detector sizes are modest. We will not tax the engineering skills of the community in building this detector. However, it must be started soon. We hope that the PAC will authorize us to proceed so that we can muster the necessary people and resources to begin testing prototypes in 1988. We intend to be ready for first physics runs when the hyperon beam in P Center becomes available after the next fixed target running period.

I. INTRODUCTION

This past year has seen significant progress in the understanding of charm hadroproduction from the experimental basis. Further results from the Fermilab and CERN fixed target programs have established the short lifetime of the Λ_c^+ baryon,⁴ confirmed the difference in D_s^+ production from π and K beams,⁵ and confirmed the existence of the Ξ_c^+ baryon.³ From both hadronic experiments and e^+e^- annihilation data has come new evidence of the Ξ_c^{++} and Ξ_c^0 baryons.⁶ Nevertheless, the baryon sector remains largely unexplored. There is rich potential for physics understanding in charm baryon decays. Because there are three quarks involved in the baryons, the opportunity for suppression effects, enhancement effects, and other wavefunction modifications of the simple spectator charm decay diagrams is much greater in baryon studies than in the meson case. To probe these effects will require an extensive data set correlating different decay modes of different baryons. The simplest example to draw concerns the lifetime ratios of the different states. Because of the enhancement/suppression effects various authors have proposed an ordering of baryon lifetimes. There is general agreement that the Ω_c^0 should have the shortest and the Ξ_c^+ the longest.⁷ The order in between is in contention. Data on these states are sparse. The Ξ_c^+ lifetime is measured to be $4.2_{-1.5}^{+2.0} \times 10^{-13}$ sec.³ Is this long like the D^+ or short like the D^0 ? The errors allow for either possibility. Clearly more data are needed to answer even such a rudimentary question. No evidence for the Ξ_c^0 , the neutral partner of the Ξ_c^+ , exists, and evidence for the Ω_c^0 is weak.⁸ The data set for Ξ_c states is very sparse. Samples contain tens of event, whether from e^+e^- or fixed target experiments.⁶ Thus, despite the new experimental information, no significant attack on understanding the underlying questions of charmed baryon decay

mechanisms can yet be made.

In all cases only one or a few decay modes have been observed for the baryons, and there is only sketchy evidence for any of the excited states.⁹ While the Mark III spectrometer at SPEAR has produced a detailed understanding of the Cabibbo favored and unfavored branching ratios of the D meson family, no such data base exists for the D_s family of mesons or any of the baryons.¹⁰ In order to establish Cabibbo-unfavored modes, one must have a large data sample of fitted events with good particle identification to minimize ambiguities.

Perhaps the most important reason for going to large-x production is that there may be new physics there. As discussed in the letter of intent, the WA62 experiment at CERN observes a much different x-distribution for Ξ_C^+ production from the Σ^- beam than is observed in E400 at Fermilab from the neutron beam. Despite the comparable number of events in the Ξ_C^+ mass peak, the x distributions are totally different, as can be seen in fig. 1. The number of interactions recorded in the two experiments were comparable, yet in a smaller x bite in a presumably less-favored part of the x distribution the lower energy experiment had a similar number of events and a similar cross section. This should be explored. Similar differences in production at different x regions seem to hold true for the Λ_C^+ . From central region experiments like NA27 Λ_C^+ physics has emerged only with difficulty.¹¹ At the ISR there have been difficulties of the opposite sort. Λ_C^+ events are seen clearly, but with anomalously large cross sections, perhaps caused by having to extrapolate from a small acceptance region to all of phase space. Now, the latest analysis shows a leading $(1-x)^2$ behavior of the invariant cross section $E \frac{d^3\sigma}{d^3p}$ and a cross section of 30 μb .² This result tends to support the idea that there are different mechanisms for charm production in different x regimes. If one considers simple quark model diagrams for charm baryon production by nucleons

and by hyperons, as shown in fig. 2, one can also think that there might well be dependences on the incident particle. While it is always dangerous to place too much significance on simple diagrams like these, we do think that they illustrate the importance of making a systematic comparison of charm baryon production from different beams at large x , where valence quark effects are the most prominent. SELEX can employ a variety of beams and beam energies to explore these matters.

A second reason for preferring large- x production over central production has to do with the difficulty of determining whether given decay modes contain two-body resonant substructure or not. Because these charm states are produced with masses not greatly larger than the charm quark mass itself, the Q values of the various decays are not large. Consequently, two-body resonances which form between final state particles may be due either to final state interactions or to the primary quark fragmentation. The low Q value will distort resonant mass distributions, because the high mass portion of the Breit-Wigner may be kinematically suppressed. Figure 3(a) shows the Dalitz plot for WA62 data. No obvious resonant structure is seen. Figure 3(b) shows a purely resonant decay of the $\Xi_c^+ \rightarrow \Sigma^+(1385)K^*(890)^0 \rightarrow \Lambda^0 K^- \pi^+ \pi^+$. Even in the Monte Carlo simulation one is hard-pressed to see any two-body substructure despite the fact that the input was pure resonance. While the Dalitz plot may not show structure, the relative branching ratios of states with zero, one or two π^0 s would be predicted uniquely for resonance domination of the decays. However, in order to measure these branching ratios well, one must have excellent geometric acceptance for all decay modes over the full Dalitz plot. In our opinion, this is far easier to achieve in a large- x apparatus. The charm state at large x is well separated from the majority of particles from the underlying event. While this separation may not be essential to do physics with all-

charged modes in detectors with silicon vertex systems, it is important when trying to analyze modes with single or multiple π^0 s, to reduce ambiguities. In addition, the $\pi/K/p$ identification will eliminate ambiguities in making resonant submass analyses of the charm decays - important for making the decay mechanism analysis that we propose here.

In order to separate baryon from meson events in present spectrometers, one must rely frequently on kinematic fitting of tracks from the observed secondary vertex. For Λ_c^+ events there is always the question of confusion with D or D_s mesonic decays. Threshold Cerenkov tagging for baryons has potential for confusion because the threshold counters used in present experiments tend to separate π from (K,p). Therefore, the confusion of K^+ and p overlaps meson and baryon states in a large fraction of events. For present experiments the criterion of unambiguous kaon identification by threshold counters limits the study of the Cabibbo-suppressed decay $D \rightarrow K^+K^-$ to a very narrow x range.¹² A reasonable way out of this confusion is to use a Ring Imaging Cerenkov Counter (RICH). Such a counter greatly extends the range of unambiguous particle identification by asking at what angle the light is emitted, not only whether or not there is light. These counters require a 2-dimensional readout to work best. A large-sized counter of this type exists in the Omega spectrometer at CERN¹³ and a similar device is being readied for use by E665. These large-area counters are a challenge to build, and efficient UV photon readouts are not easy to maintain. However, by limiting the angular spread of the particles to be identified, as is proposed here, the detector problem is greatly simplified. We can use photomultipliers. SELEX aims at full particle identification (π, K, p) over the whole momentum range of interest for large-x charm baryons. This is the third reason for preferring large-x over central production for these kinds of studies.

A fourth reason for preferring large-x production is the opportunity that it offers for using the longitudinal development of the secondary decay to aid in event recognition. This experiment will introduce the use of silicon pixel devices for charm identification.¹⁴ At large x the flight path of the charm state can be long enough to bring it close to a pixel detector. In a multi-prong decay one can then compare the charge seen per pixel with that expected from the silicon vertex detector (VSSD) reconstruction of the event. In central production flight paths tend to be too short to exploit this method to advantage.

Despite the emphasis on large-x physics, we must hasten to point out that SELEX has good acceptance and triggering over an x range from 0.1 to 1.0. As such, it is unique among charm spectrometers, existing or proposed, in its abilities to study the transition from central to leading production. The triggering can be adjusted to favor one region over the other by software. Thus, physics results can lead to rapid experimental response to follow interesting effects either into the large-x or small-x regime. This flexibility is important in a second-generation charm experiment. We should also note that the emphasis here is on baryons, because we perceive that field as the less-well-understood. However, SELEX can do a superb job of exploring meson physics as well, if there remain open questions in D_s physics, for example. The particle identification arguments made for baryons hold equally well for mesons. The forward RICH can operate with different gases for different purposes. Magnetic fields can be adjusted to transmit different momentum ranges, and the trigger matrix retuned to select different configurations as needed.

To compare SELEX to the existing charm spectrometers we show in table I the proposal numbers for charm events anticipated in E769 and E687 (photon beam).

For SELEX we have cited only the baryon yields. Meson yields will also be large, but for the most part meson physics will have been done elsewhere, as we see it now. As you see, the potential yield in this second-generation experiment far exceeds the sample sizes expected in the near future. Thus, we will be in position to look at physics on beyond the first hints of charm production characteristics.

TABLE I

PROPOSAL ESTIMATES OF CHARM YIELDS

| EXPERIMENT | TRIGGERS RECORDED | CHARM RECONSTRUCTED | X RANGE |
|-----------------------|--------------------|-----------------------------|--------------|
| E769 | 0.3×10^9 | 6500 (mesons) | -0.05 to 0.8 |
| E687 (γ beam) | 2×10^9 | 1.5×10^6 (mesons) | -0.05 to 0.8 |
| P781 | 6×10^{10} | 1.5×10^6 (baryons) | 0.1 to 1.0 |

II. PHYSICS GOALS

A. STUDY OF CHARM BARYONS

This objective, the primary one of the proposal, has been outlined thoroughly in the introduction. We shall be brief here. The aim is to make a systematic survey of charm baryon production and decay mechanisms. Such a data set is needed to understand if perturbative QCD can account for charm production under different circumstances and to establish which mechanisms dominate decay processes. By having complete particle identification for hadrons, electrons, and gammas, one can normalize branching ratios to the semileptonic rates. This aids the theoretical analysis of the hadronic modes. The ability to measure π^0 and η^0 states is also important in analyzing these ratios for evidence of resonant substructure. This substructure is clearly the dominant feature of meson decays.¹⁰ It was not expected.¹⁵ Now that experiment has demonstrated the effect, there are models which do an excellent job of matching the data for mesons.¹⁶ The analysis for baryons is somewhat more difficult, but initial efforts to understand Λ_c^+ decays have been made.¹⁷ Further progress in this area will await new data.

The semileptonic modes are especially important in understanding the question of suppression or enhancement of hadronic decays. If the semileptonic rates are not influenced by the various mechanisms which affected the overall lifetime, then measuring the relative branching ratios of different charm baryons, normalized to their semileptonic rates, is sensitive to wave function effects in the decays.

Finally, we are interested in measuring correlation effects in charm baryon production. It is especially interesting to see if there is a change in the correlation as one goes from small x to large x , as well as to compare meson

correlations with baryon correlations. In SELEX the trigger is on the large-x system. However, the acceptance is quite good for slower partners if there is a positive correlation, i.e., if the mass of the $c\bar{c}$ system is not too large or if the color attraction of one c quark to a spectator system is not too strong. If the Σ_c^+ cross section at large x is as large as reported by WA62, then the production rate is high enough to make a full-acceptance correlation study by using an emulsion target. This would give a complete picture of the correlation. We estimate that a 10-liter emulsion exposure would supply several hundred Σ_c^+ events. Some members of the Japanese emulsion group have expressed an interest in this possibility.

(B) SEARCH FOR NEW BARYON STATES

As has been mentioned earlier, three of the expected ground state charm baryon multiplet essentially have not yet been seen: Σ_c^+ , Σ_c^0 , and Ω_c^0 . There is a 3-event clustering in WA62 data suggestive of the Ω_c^0 decay.⁸ We expect to acquire a large data set containing various decay modes of all three baryons. The Σ_c^+ decay, whether by γ or π^0 , to Λ_c^+ is difficult to detect. The de-excitation particle is slow, emitted along the baryon line of flight. For γ decays, this means that one must find a low energy photon at 0° - a formidable job. We expect to do that in SELEX by having a finely segmented liquid argon calorimeter far from the target, so that such photons can be separated from the bulk of the primary interaction π^0 decays. The photons from the de-excitation π^0 would be at wide angles in $x \sim 0$ baryon decays. However, the Lorentz boost from a large-x baryons sends the π^0 forward into the downstream LAC or Pb glass arrays. The segmentation there is fine enough that the average occupation probability of a given cell is low. That is what is needed to pick up these gammas with good efficiency. Thus, large-x production offers significant advantages in searching for excited states of the ground state multiplets. The

soft decay particles emerge in regions sparsely populated by products from the underlying event.

(C) SEARCH FOR EXOTIC STATES

The search for 4-quark mesons has been a frustrating experience for many groups. However, the observation of a candidate state, the U meson, in WA62 necessitates some further study.⁸ This high mass meson has unusual flavors in its decay modes, especially $U^+ \rightarrow \Lambda^0 \bar{p} \pi^+ \pi^+$. This makes it a good candidate for the RICH trigger mode discussed in the trigger section. In general, online selection of unusual flavor combinations can be made for large-x states, permitting an efficient trigger for exotics that could be mixed in at low rate with triggers from the major interest areas in the experiment. Such a flavor-tag is straightforward only in large-x systems, in which all tracks from the exotic state are folded into the particle identification system.

(D) STUDY OF CHARM PRODUCTION MECHANISMS

There are several hints in the systematics of charm production that various charm states are flavor-dependent in their production. For meson systems E769 is pursuing suggestions that D_s mesons are produced differently from K beams than from π beams. We have alluded to hints from E400 and WA62 that Ξ_c^+ states appear to be produced differently from n and Σ^- beams. In P Center the hyperon facility can readily supply hyperon, p, n, and π beams to the SELEX apparatus. This allows a variety of QCD studies to be made, not only on charm systems but on heavy strange states like Ξ^* and Ω^* as well. Then there is the question of A-dependence. E769 has made the case well for using different target materials in a high-statistics study to find any x-variation of the A dependence in charm production. We plan to pursue the same general program for charm baryons. With statistics like we expect, the details of x-variation in different materials can be well-mapped.

(E) STUDY OF BEAUTY PRODUCTION

The question of detecting beauty states, mesons or baryons, is a major issue at Fermilab currently. In SELEX we are, of course, interested, but it is hard to guarantee a result. However, there is one major area of beauty studies in which SELEX may contribute. Because of the ability to tag electrons in the TRD and also at the same time to calculate their upstream angle and their momentum, SELEX can implement an electron p_T trigger. Thus, the standard SELEX trigger structure is perfectly set to tag semileptonic decays of B particles. These modes are among the most useful experimentally, since they are expected to have 12-15% branching ratios. No other single B decay mode is likely to be this large. Thus, even though the SELEX apparatus is not designed to handle the extraordinary rates planned in E771, the B detection capability is not negligible. As discussed in section VI, the standard trigger will select ~100 B particle (meson or baryon) decays to $e^\pm \nu X$ in the first run.

III. BEAM AND TARGETS

The Proton Center hyperon facility provides a variety of beams which can be brought to the SELEX spectrometer. At a secondary momentum of 600 GeV/c it can provide a negative beam that is about 50% E^- , 50% π^- 10m downstream of the production target. Beam tagging by a TRD system gives very clean E^- or π^- selection, as shown in fig. 5. Positive beams (30% π^+) of comparable momentum will give protons of any desired energy up to the highest momentum allowed by radiation safety limits (~750 GeV/c). A good quality neutron beam has also been used already in this area. (E630)

Detailed flux information on hyperons is available at 400 GeV incident energy. Comparisons with CERN indicate that fluxes scale well in x and p_T . Flux data are being taken now in E756 for 500 GeV secondaries from the 800 GeV beam. While particle ratios are not yet available, the total flux has been

measured. To produce a secondary flux of 2×10^6 negative particles/second takes 1.6×10^{10} incident protons. Thus, for a 20 second spill we would ask for 3.2×10^{11} protons, a light load on the accelerator. For P781 we would reconfigure the hyperon channel to have a smaller momentum bite and raise the beam energy to 600 GeV. The incident proton flux would go up correspondingly to about 5×10^{12} . The muon flux will probably restrict further flux increases for negative beam even though the target station could handle more intensity. For positives or neutrons this limit would not pertain; muon background would be a 10% effect.

For each of the possible secondary beams, the exit beam profile would have a spot size of order 0.5 to 1.0 cm^2 , divergence of order 1 mrad, and flux, including muons in the beam, of order 2 MHz. The muon background in this area is rather broadly dispersed. Most of the muon flux comes from channeling through the Al coils of the hyperon magnet, rather than directly through the hyperon channel. The muons are not a serious problem for the silicon detectors in the apparatus. They are most troublesome for the large area drift chambers.

The targets must be arranged to satisfy several requirements for the apparatus. It must be possible to reconstruct the primary interaction point fast and accurately. We want to measure particle lifetimes in the range from 0.1 to 1.5 ps. This requires excellent vertex resolution along the beam direction and low multiple Coulomb scattering after the decay. Many of the considerations along these lines are spelled out in the E769 proposal. Because A-dependence of charm baryon production will probably still be an important issue for SELEX, we plan to use different materials in the target string. Each foil will be of order 1mm or less in thickness to permit fast reconstruction of impact parameters, as discussed in the trigger section. We intend to operate with up to 5% interaction length total in the target foils, with up to 10

foils, depending on material. Targets will include C, Si, Cu, Ag, and W.

IV. SPECTROMETER

SELEX is planned as a multi-stage spectrometer, expandable to cover different physics regimes as needed. The initial goal is the study of large- x physics for baryons, as outlined above. Even at this stage, however, it is necessary to supply coverage for a great many small- x particles, since resonant states produced in heavy flavor decays may give their decay products appreciable momentum into the backward hemisphere. Consequently, SELEX is designed with a large-acceptance first stage, very similar to that now seen in $x \sim 0$ spectrometers. This stage sweeps out many of the prongs from the underlying event before they enter the trigger region after magnet 2. It also picks up de-excitation pions from excited baryon or meson states, so it is crucial to the major goal of the experiment to have this large acceptance. Of course, the heart of the experiment is the high resolution high-momentum spectrometer and the subsequent trigger and particle identification systems. It is this part of the apparatus that allows SELEX to be selective, to aim for 10^{11} interactions per run, rather than the 10^9 limit now achieved. We consider each part in turn. The spectrometer layout is given in figure 4. Table II shows the number of channels and the sizes for all detector systems.

a) beam system

The beam spectrometer is designed to measure the incident beam trajectory to a precision of $3\mu\text{m}$ in x and y , using $20\mu\text{m}$ pitch silicon strip detectors (SSDs). This resolution has been achieved by several groups at CERN, using conventional electronics and also, in a recent report, using AC-coupled readout electronics to reduce the influence of leakage currents on position resolution.¹⁸ These systems must have analog and digital readout.

The beam flux through the detectors is high, ~ 2 MHz, but well-dispersed.

Radiation damage will not be a problem. Assuming a relatively uniform flux distribution in the 0.5 cm² beam spot, the lifetime of the SSDs should exceed four years of operation. The readout electronics must be designed for fast charge collection and shaping. Present CERN electronics or LeCroy preamplifiers are quite well-suited for this purpose, as are new circuits being developed at Fermilab. We expect that the silicon detectors will measure the incident Σ^- and π fluxes on a particle by particle basis with no pileup problem. We intend to veto any events with two beam particles in the software trigger, since it will cause too much confusion. The muon admixture in the beam area is too small to cause difficulty.

The beam particle identification problem is the separation of Σ^- from π^- . The admixture of other hyperons is too small to be of concern at the large x of this beam operation. The K^- flux is also negligible. Consequently, a transition radiation detector (TRD) system will work very efficiently to separate Σ/π . The problem is to make it fast enough. In the design presented here by the Leningrad group, the charge collection is done in 100 ns. The separation curves for the proposed design are shown in fig. 5 for equal fluxes, as is the case here. There will be beam scintillators for timing and beam envelope definition. They are not shown here.

The other major piece of the beam system is after the target, viz., the interaction silicon wafers. This pair of silicon wafers is designed to provide a fast (50 ns) signal indicating that three (3) or more charged prongs traversed them in coincidence with an incoming beam track. Other experiments have used these detectors for interaction counters; they work reliably and introduce little extra mass.

b) vertex pixel detectors

One of the newly-developed detectors that will be installed in P781 is a

silicon pad detector. This device is being tested now by a SLAC/LBL collaboration.¹⁴ In our application it will use a $30\mu\text{m} \times 30\mu\text{m}$ pixel pattern in a square array of 256×256 cells. The $300\mu\text{m}$ thick chip is Indium bump-bonded to a second $300\mu\text{m}$ silicon wafer containing the readout electronics. The readout is charge-storage, with each cell being randomly addressable. Thus, pattern information from downstream detectors can be used to reduce the number of pixels which must be digitized. The readout chip is available in small quantities now. The $30\mu\text{m}$ pixel unit has been fabricated already in Ge and operated for astrophysics purposes.¹⁹ A Si version is now underway. This device will be used for offline analysis to supply data on the number of particles located within one $30\mu\text{m} \times 30\mu\text{m}$ region near an alleged secondary vertex.

c) vertex silicon strip detectors

In 1987 detailed explanations of SSDs are no longer needed. In large measure, the widespread availability of SSDs is responsible for much of the progress in charm physics over the past two years. For P781 the new features in second generation silicon applications are the attacks on readout costs and readout complexity made possible through the VLSI Microplex approach. In present systems preamplifiers are major cost items. The readout costs far exceed the cost per channel of the detector itself. Those systems using analog readout for increased spatial resolution and double-hit detection have large investments in FASTBUS or other high density analog-to-digital converters. For the past several years work at SLAC, LBL, RAL, MPI/Munich and other laboratories has aimed at using VLSI technology to integrate 128 preamps onto a single readout chip. The more ambitious designs (LBL) even include digitization, memory and editing functions on the same chip. Various chips are needed for e^+e^- physics in 1989 and for CDF on the same time scale to

serve as vertex silicon readouts. The designs were originated for collider physics, in which the bunch crossing timing is well-known. In P781 we must see if they can be adapted to fixed target work at the rates we need. At present there are at least two chips which look promising. The MPI/Munich chip has a switched-capacitor memory clocked externally. For a fixed target experiment, one stops the clocking for events of interest. In the present version (NMOS) this chip is too slow. However, a CMOS version is in preparation; that will almost certainly be fast enough to handle the 50 kHz interaction rate in SELEX. The LBL chip, with its increased function at comparable cost, is also possible. Its strobe delay of 220 ns makes it possible to strobe it on the interaction signal, a 50 kHz rate. That is fine. The remaining uncertainty is how to manage the double correlated sampling when one does not know the event time in advance. Several possibilities are being explored with LBL. To summarize we believe that the situation will stabilize within the next year and that microplex readout chips of suitable speed and timing sequence will be available by 1989 for SELEX applications.

The silicon detectors themselves are also of a new type. One of the problems seen in present vertex silicon applications is the multiple Coulomb scattering in the detector elements themselves. This affects extrapolations to find impact parameters, for example. It also converts photons in the VSSD, making extra tracks. Various suppliers are now producing prototypes of double-sided SSDs - detectors in which both sides of the diode detector have readout patterns. These detectors, implemented on 200 μ m Si, offer greatly reduced scattering and conversion. In SELEX, going to high momentum reduces the scattering problem anyway, but having double-sided detectors opens the very crowded vertex region for easier access, better mounting and surveying, and other detectors. This step will again improve function and lower cost.

The detector details given in Table II are quoted for 150 mrad coverage. This angular range is wider than required for studying forward charm production. It will encompass a large fraction of two-charm production in the forward hemisphere. Because the detectors themselves are relatively cheap, we have taken the suggestion of the PAC after the Aspen meeting and have shown full angular coverage in the VSSD system from the beginning.

d) slow particle spectrometer

After the first weak-field ($\Delta p_{\perp} = 0.3 \text{ GeV}/c$) magnet M1, a drift-chamber spectrometer is inserted to pick up the slow tracks from the backward hemisphere of large-x charm particles. As discussed in the letter of intent, decays via two-body resonance substructure can disperse decay products over an even larger angular range than is the case for phase space decays. Thus, this region is important for decay mode studies. This is also the region of the detector in which de-excitation π^{\pm} from baryon (or meson) excited states will be detected. This part of the system resembles any central-region charm spectrometer now on the floor.

Because we must measure particles in the same phase space region as the beam and because the hyperon beam is large, the centers of all drift chambers in this region must be deadened. We cannot afford to give up this forward information, so 50 μm pitch SSDs are mounted on skeletal frames to give high-resolution measurements in the central 5 x 5 cm^2 . The detectors and lightweight mounts are connected to an external frame outside the active region of the drift chambers. Only line-driver electronics is mounted on the wafer, and signals are sent out over Kapton printed circuits to minimize the mass presented to particles going outside the acceptance of the silicon. In this way the large-x baryons are measured with 15 μm accuracy in the silicon, while the slower, wider-angle mesons are measured with 150 μm precision in the

drift system. The SSDs can handle the beam rate with no problem. The drift chambers see only the much lower interaction rate, dispersed over a much larger area. The number of readout channels in the system is given in Table II.

e) wide angle Pb glass array

One of the goals of this experiment is to study a complete set of baryon decay modes, including those with π^0 s. For backward-hemisphere π^0 decays the photon lab angles go out to 100 mrad. The photon density in the angular range 30-100 mrad is not too large, based in E653 data for 800 GeV proton interactions, < 10 photons/event. A Pb glass array of several hundred blocks is well-matched to this problem. These photons will tend to be soft; Pb glass has good low-energy photon efficiency. The shower sizes will tend to match Pb glass array sizes. Pattern recognition is not expected to be severe in a pixel system with low occupancy per cell on the average. This array will give good reconstruction efficiency for wide-angle π^0 s and will view the target through the low-mass drift chamber active volume and the 4% of a radiation length of silicon in the VSSD.

f) fast particle spectrometer

The particles of chief interest in this experiment are small-angle high momentum tracks that traverse the second dipole M2 ($\Delta p_t = 1$ GeV/c) and are tracked in a second set of drift chambers spread over 2 meters. The beam is still too intense for unprotected drift chamber operation. The central region is covered by silicon mosaic detectors of the sort used in E653. This gives excellent tracking for the highest momentum particles, for which drift chamber resolution and two-track separation is not good enough. The remaining tracks are well-measured in the drift system.

For triggering purposes 8 2mm spacing PWCs (4 X, 4 Y) are interspersed in this region. They play a crucial role in reconstructing tracks online in the

trigger processors. These chambers are of conventional size and construction. The beam is dispersed over several wires, so the rate/wire doesn't exceed 500 kHz. The tracks recognized in the PWC system will be followed into the drift chambers in offline processing for optimal mass and momentum resolution.

g) electron transition radiation detector

The idea of triggering on electron p_t as a beauty signature has been mentioned in the introduction. In order to do that, a highly-segmented electron detector must be used in a relatively low-rate environment. In SELEX one can use the proven device built for E715, set downstream of the tracking region. In this way track segments located in the PWCs can be checked for TRD photon clusters along the expected trajectory to flag electrons track by track. Electron-hadron rejection is very good ($\sim 1000/1$ offline with 90% electron efficiency). This device gives us the very important handle on tagging the semileptonic decays of heavy flavor states.

h) ring-imaging cherenkov counter

The RICH is one of the major systems in SELEX. We rely on good particle identification over the whole kinematic range transmitted by M2 (30-600 GeV) to look for structure in the different baryon decay modes and, in some cases, to implement a flavor-tag in the trigger. The problem for the RICH is to cover a wide momentum range, to have good π/K separation up to 250 GeV/c, and to produce enough photoelectrons to have high efficiency. As discussed in the letter of intent, the solution we have chosen is to use a photomultiplier matrix. This has the advantage that the quantum efficiency is a well-known, large number ($\sim 17\%$ averaged from 300-550 nm). The output signal is easily digitized with PWC amplifier-discriminator units to give a pixel-readout and is available at trigger-decision time. The only question is how many phototubes are needed.

For SELEX the angular coverage is limited by the transmission through M2 to ± 20 mrad vertically and ± 65 mrad horizontally. For a Ne radiator, one expects 1.3 photoelectron/m; we have designed a 10m counter to compensate the packing losses of mounting 15mm phototubes with 10mm photocathodes in a hexagonal close-packed array. Winston light cones allow one to exploit the limited angle range to improve photostatistics. There should be 9 photoelectrons on average. With a noble gas fill, chromatic aberration is small and detector resolution determines the ring diameter resolution and hence the π/K separation limit. With these phototubes, the π/K separation is 1.2σ at 250 GeV/c. 2800 phototubes are required.

1) VEE decay detectors

In a baryon experiment Λ^0 triggering is an essential aspect. For the high momentum Λ^0 s in SELEX the opening angle of the VEE is a few milliradians. Thus, the angular region covered by these chambers is determined chiefly by the angular range of interest for the Λ^0 s themselves, about 10 mrad. Even at the end of the decay region at 35 meters, the chamber sizes are modest, of order 80 cm square. As discussed in the appendix on triggering, we will look for charge jumps of two units between the center region of the upstream member of a chamber pair and the full area of the downstream member. Because the mean charged particle occupancy of these chambers is low after the sweeping of the two dipoles, this charge jump is a characteristic event and should have very little background. Λ^0 momentum accuracy is $\sim 5\%$ from opening angle alone in this system. One wants to do better, so most decays will have at least one particle momentum-analyzed in M3, a large-aperture dipole at the end of the decay region. The chambers in this region are a combination of a PWC for triggering and (X,X',Y,U) drift chamber modules for tracking resolution at each station. Wire counts are given in Table II.

j) forward Pb glass array

The need to measure neutrals well has been discussed earlier. For de-excitation π^0 s from baryon (or meson) excited states, a Lorentz boost of 150-300 can be expected from large-x production. This means that the π^0 decay angles will be a few milliradians for symmetric decays, tens of milliradians for asymmetric ones. The downstream photon detectors cover the forward 30 mrad aperture left open in the upstream Pb glass detector. Because this forward array is 34 meters downstream of the target, the blocks can be relatively coarse and still subtend a sufficiently small solid angle to have low occupancy probability. The Pb glass, mounted in front of the Λ^0 analyzing magnet, covers the range 7-30 mrad.

k) liquid argon calorimeter

The forward region is covered by the E653 liquid argon calorimeter. This has the advantage of excellent pattern recognition capability, thanks to a strip and pad geometry for 2d shower reconstruction. The problem in the forward direction is to separate soft photons from excited state transitions from the diffractive π^0 decay photons. The transition photons will be Lorentz-boosted from the range 50-130 MeV to the range 7.5-40 GeV. Single photons in this energy range will show up well in the LAC. They will follow the parent charm particle's line of flight, so they will be separated from the beam by ~6 cm at the LAC position. This means that one can modify the LAC to include a beam hole without giving up a critical region of photon phase space. Such a modification may be necessary to handle the high beam rates in SELEX. That is a detail. The main point to be made is that this LAC will give excellent position information about shower origins at 42 m from the target, so the angular precision, crucial for π^0 reconstruction, will be unmatched. Also, the long lever arm will help to separate showers in the forward direction and

aid in the analysis of modes with multiple neutrals. Only π^0 candidates in certain regions will be able to balance p_t in the event relative to the observed primary and secondary decay vertices. A fine-grained detector helps to reduce the ambiguities in such circumstances.

1) neutron calorimeter

For handling the Cabibbo-suppressed decays of charmed baryons and also for identifying Σ^- decays which occur part way through the system, neutron detection is a very important element. The existing neutron calorimeter from E497 is a reasonable match to the SELEX system. It covers the central 5 mrad cone, a good match for large-x production. The timing signal from its scintillation counters can go to the first-level trigger as needed. The neutron interaction point information from the PWC readout will give high precision neutron angle information, and the calorimeter normalization will measure the energy to $\sim 100\%/\sqrt{E}$. At 250 GeV neutron energy, this would be a 6% energy measurement. This is good enough to be useful for testing reconstruction hypotheses.

V. TRIGGERING

(a) Introduction

One of the major advances needed in progressing to a second-generation charm experiment is the implementation of a "charm trigger". We define this as a selection process which retains a large fraction of charm in an arbitrary decay mode while rejecting non-charm background interactions at the 100:1 level. First generation charm experiments have used triggers with enhancement factors of order 5. To do appreciably better, we must aim for at least a 10-fold improvement in the triggering.

Complicating any trigger design is the large variety of decay modes and lifetimes expected for charm baryon decays. We have concentrated on trigger

schemes to work on the hardest problems, those of short-lived states like the Λ_c^+ . We expect that detecting the longer-lived states will only be easier. For SELEX we want to use only software-controlled trigger schemes. It may be necessary to employ a few different first-level triggers, as outlined below. If this is the case, then we want to be able to switch between them without hardware modification. In order to do a search not only for charmed particles but also to do some of the production experiments mentioned in the introduction - especially searches for exotics - one wants to use the RICH tag online to select exotic particle combinations like double-strange or strange antibaryon systems. This requires computation to predict the Cerenkov ring position for online comparison. In SELEX the emphasis of the trigger design is to introduce tracking and online computation at the earliest possible stage and to use the minimum possible set of hardware constraints.

(b) Charm Triggers

Among the most difficult problems for charm triggers is the set of low-multiplicity, short-lifetime modes characteristic of the Λ_c^+ . A large branching ratio is expected for modes like $\Lambda_c^+ \rightarrow \Lambda^0 + \pi^+$. The corresponding Cabibbo-unfavored mode would be $\Lambda_c^+ \rightarrow n + \pi^+$. These "kink" modes put the maximum strain on the first-level trigger and so have received special attention. The Λ_c^+ lifetime is short. Recognizing a "kink" close to the primary vertex is even harder for it than for a longer-lived state like the D^+ . The only trigger that we have been able to imagine that will meet all the demands posed by these modes is an impact-parameter trigger. Any heavy-flavor decay has a nonzero impact parameter b , however small it may be. Its magnitude is essentially x -independent. This trigger will handle the Λ_c^+ one-prongs with good efficiency. Other modes that we have studied are also tagged well by this scheme. Therefore, we propose it here as a general purpose, high sensitivity charm

trigger capable of operating over a large range of x . It requires the ability to reconstruct "interesting" tracks in the vertex silicon detectors with full resolution in real time, i.e., prior to the next beam spill. The ability to achieve this kind of computation speed and preserve full vertex silicon resolution ($\sigma_b=6\mu\text{m}$) now appears to be at hand. This makes P781 possible.

The idea of an impact parameter trigger is, of course, not unique to this proposal. WA82 at CERN is now using an impact parameter trigger to study central production from 300 GeV π and p beams. With a $100\mu\text{m}$ projected impact parameter cut on tracks with >4 GeV/c momentum they achieve a trigger reduction factor of 40 over pure interactions. Offline, the WA82 silicon vertex detector achieves an impact parameter resolution on the primary vertex of $10\mu\text{m}$. Their vertex region layout is shown in fig. 6. Charm meson systems, of course, have lifetimes much longer than expected for some charmed baryons, e.g., Λ_c^+ and Ω_c^0 . In order to trigger efficiently on systems with lifetimes of 0.15 ps, rather than 0.4 ps, it is necessary to improve the vertex cut from $100\mu\text{m}$ in projection to of order $20\mu\text{m}$ in space. SELEX intends to do this. It is an ambitious goal. The discussion in Appendix I outlines the method in detail. We summarize it here.

The scheme depends on the filtering effects of the two magnets to select a fraction of the tracks from the primary interaction to be analyzed for charm.

There are four levels:

- fast scintillator selection;
- downstream track segment reconstruction;
- upstream track segment and vertex identification;
- full 3d reconstruction of these tracks to compute impact parameter.

The first level uses the charm enrichment of the set of positive tracks from a negative incident beam to suppress non-charm interactions. Level 2

reconstructs tracks to allow projection downstream into the RICH and upstream into the vertex silicon detectors (VSSD). Level 3 tracks the small angle, high momentum tracks which have a good chance of coming from a large-x charm decay to a primary interaction in one target foil, using beam information. Level 4 then computes the interaction point and tests each of the tracks for an impact parameter of at least 2.5 standard deviations. We expect to gain a factor of 20 in non-charm background suppression with this real-time computation with an efficiency of 0.4-0.8 for charm events. As the efficiencies presented later indicate, this seems to be possible. The trigger logic must contain a number of powerful computing engines, of order 100 ACP modules of the present generation. A possible data acquisition architecture for P781 is being studied using a new set of processors just now appearing in the market. This would be more compact but functionally equivalent to an ACP farm. We will use this newer approach if it is ready, because it is more cost-effective. However, either scheme approaches the problem in the same way - add enough nodes to be able to feed one event to a given processor and let it compute the necessary event parameters to reject or accept that event. As long as there is enough space in event memories to hold an entire spill's worth of data, then one has 50 seconds to process the events and write them to tape. In our case, the decision time on a VAX 8600, using a straightforward algorithm to reconstruct and reject real data from 800 GeV p-Carbon interactions with 11 tracks per interaction (average), is < 5 ms/event. The input event rate is 10 kHz, or 2×10^5 events to process. With 50% bus efficiency and 20 8600-scale processors (120 ACPs) we need 50 seconds to handle the data. We are confident that the algorithm can be made significantly faster. We are also sure that the computing requirements will grow more complex, to cancel any gains. However, the point to be made here is that the scale of computing needed to implement

the impact parameter computation for the charm-enriched set of tracks downstream of the second magnet can be managed with 1987 technology at reasonable cost. This approach is practical.

The steps in the trigger are detailed in Appendix I. The scintillator-based first stage uses the fact that the charm baryon states of interest have charges which differ from the beam charge by one, two, or three units. Therefore, for large-x production one can expect to see more fast "wrong-sign" particles from charm events than one would from normal interactions. Moreover, because the Cabibbo-favored decays involve a $c \rightarrow s$ quark transition, there should be strange particles in the final state. Thus, we emphasize a fast VEE trigger and a trigger selecting two fast positive tracks from the Σ^- beam. This selection is imposed by a trigger matrix after the second magnet, set to accept tracks with slopes corresponding to high momentum positives. The VEE decay space is a 26 m drift region after this magnet, in which one looks for charge jumps of 2 within a 10 mrad cone angle. Any fast Λ^0 s from charm baryon decays will be within this cone, but most of the forward charged secondaries will have been swept out of it. Details are again in the appendix.

In order to find evidence of charm decays we must reconstruct the primary interaction vertex to good accuracy and link tracks to it. To do this for every track in the primary event is too computation intensive. Because we emphasize large-x events, the tracking is done only for those tracks which go through the second magnet. This is a charm-rich sample, and in every good event one or more of these tracks should have a nonzero impact parameter. The first step in finding them is to reconstruct the downstream segments. These straight lines are found in sets of four 2mm PWCs for X and Y tracking after magnet 2. The hits in these chambers are fed to the processors from the event memories as soon as a processor is free. The computer finds track segments

with 3 or 4 hits and checks to make sure that there are two "wrong sign" fast tracks, or one wrong sign track if there is a VEE. This rejects those forward diffractive clusters that look like wrong sign events to the matrix and gains a factor of 2 in background suppression.

At the next level the downstream slope and position are used to create "roads" in which to search for tracks in the vertex silicon detectors. Instead of having to run a general tracking algorithm among the many hits in these planes, we only search along a narrow (± 1 mm) path at a specific angle (± 1.5 mrad) based on downstream tracking predictions. This part is very fast and accurate. It finds not only the predicted track but several primary tracks as well in this search. These tracks are compared to the beam track to establish in which target foil the primary interaction took place. When this is known, the impact parameters of all tracks found in the vertex detector are computed with respect to the beam track at the center of the target foil.

Finally, in level 4 a 3d fit to each track is done, a full vertex reconstruction made to find the actual position of the vertex, and the precise impact parameter of each 3d track computed. If we can achieve the intended $8\mu\text{m}$ resolution, then a $20\mu\text{m}$ cut should reject 95% of the non-charm events. At this point the rate is 250 Hz, and we can write all remaining data to tape.

(c) Evaluation of the Trigger

In order to see the effects of these trigger stages on the various charmed baryons of interest in this experiment, we have imposed the trigger matrix on the outgoing trajectories in the experiment. We had already seen that the apertures in the experiment were large enough to give extremely high geometric efficiency over a wide x range (0.1-1.0). When a trigger matrix is imposed, it will limit the detection efficiency if a given decay mode has a momentum distribution which differs significantly from that which determines the matrix.

While this matrix is loaded by software and could be modified for different configurations, it would run counter to the philosophy of SELEX to be forced to change the matrix for every different decay mode of interest. Fortunately, this is not the case. Figure 7 shows the geometric acceptance and the matrix trigger efficiency versus x for several all-charged modes.

The cases we have studied in detail are those which should put the most varied requirements on the matrix: $\Lambda_c^+ \rightarrow \Lambda^0 \pi^+$; $\Lambda_c^+ \rightarrow p K^- \pi^+$; $\Xi_c^+ \rightarrow \Lambda^0 K^- \pi^+ \pi^+$ and $\Omega_c^0 \rightarrow \Xi^- \pi^+ K^- \pi^+$. The triggers for level 1 are either "2 fast" or "1 fast + VEE". For the $\Lambda^0 \pi^+$ decays in particular, the two triggers are complementary in their x -dependence. The triggers were examined over the x range of 0.1-0.7, i.e., from very central to very leading. The efficiency varies smoothly over the range. In the central region where the cross section is largest, the efficiencies are still of order 10% or better. Trigger differences between states with or without an additional π^0 are never very large, indicating that the matrix as implemented is not clipping very hard on the charm trajectories for $x > 0.3$. The efficiencies as quoted in Table III are quite respectable. This 4 level trigger sequence achieves the desired rate reduction from 50 kHz to 250 Hz in a way which retains almost every charm decay mode that we can imagine. For baryon states not mentioned explicitly, note that Ξ_c^0 decays will be Ξ rich, so that the "1 fast + VEE" trigger will be effective. For Ω_c^0 decays, there will be many Ξ s, Λ s, and K^- s, suggesting the "1 fast + VEE + K^- " level 3 trigger. The impact parameter is small for the short-lived states like Ω_c^0 and Λ_c^+ , but the VSSD resolution is very good. Having the beam with its large spatial size and broad angular spread traversing all the silicon detectors in the experiment gives us invaluable alignment information at any time we want it. Therefore, we have the capability to maintain the apparatus alignment to the $1\mu\text{m}$ accuracy that is needed in order to do this kind of impact

parameter trigger.

TABLE III

| Reaction | Trigger | Matrix efficiency at fixed x | | | |
|---|---------------------|------------------------------|-----|-----|-------|
| | | x= 0.1 | 0.3 | 0.5 | 0.7 |
| $\Lambda_c^+ \rightarrow \Lambda^0 \pi^+$ | 2 fast | .24 | .43 | .36 | .28 |
| | 1 fast + VEE | .00 | .21 | .38 | .50 |
| $\Lambda_c^+ \rightarrow \Lambda^0 \pi^+ \pi^0$ | 2 fast | .20 | .43 | .34 | .28 |
| | 1 fast + VEE | .00 | .16 | .34 | .46 |
| $\Lambda_c^+ \rightarrow p K^- \pi^+$ | 2 fast | .05 | .60 | .81 | .88 |
| | $p K^- \pi^+ \pi^0$ | .00 | .29 | .57 | .69 |
| $\Xi_c^+ \rightarrow \Lambda^0 K^- \pi^+ \pi^+$ | 2 fast | .12 | .68 | .71 | .73 |
| | 1 fast + VEE | .01 | .20 | .32 | .47 † |
| $\Xi_c^+ \rightarrow \Lambda^0 K^- \pi^+ \pi^+ \pi^0$ | 2 fast | .10 | .62 | .68 | .73 |
| | 1 fast + VEE | .00 | .11 | .25 | .33 † |
| $\Omega_c^0 \rightarrow \Xi^- \pi^+ K^- \pi^+$ | 2 fast | .10 | .46 | .57 | .64 |

† These two triggers are not linearly independent, so the sum of ϵ may exceed 1 for Ξ_c^+ decays.

VI. RATES AND YIELDS

The beam fluxes discussed in section III and the triggering efficiencies presented in section V allow us to compute the yield for the experiment if we know the charm cross sections. We don't. However, the body of data now in hand permits some reasonable estimates to be made. E743 reports that the charmed meson cross section for 800 GeV pp collisions is $\sim 60 \mu\text{b}$.²⁰ Using a very different technique, E400 reports that for 600 GeV nA collisions, the cross section per nucleon for A^1 dependence of charm meson production is ~ 300

μ b/nucleon.³ This gives a range within which to make estimates. Charm baryon production from baryon beams is likely to be smaller, although comparable, cross section. E400 estimates a $50\mu\text{b}/\text{nucleon}$ cross section for Ξ_c^+ production.³ WA62 measured a cross section (A^1 extrapolation) of $0.5 \mu\text{b}/\text{nucleon}$ for $x > 0.6$ at $135 \text{ GeV}/c$ in the one decay mode that they observed.⁴ For the weights given in table I from equation (2) below, that implies a total cross section of $70 \mu\text{b}/\text{nucleon}$ if the branching ratio into this mode is 5%.

In order to compute rates for SELEX from these ranges of cross section values, one must also make some statement about the x dependence. This is still an open question that will, in all probability, be clarified substantially by E769 results within the next year. However, there is substantial evidence for a two-component x distribution for heavy flavor production, both from mesons and from nucleons.²¹ In making rate estimates here, we have assumed an x distribution suggested by NA27 analyses of hadron production in 400 GeV pp collisions:²²

$$(2) \quad E \frac{d^3\sigma}{d^3p} \propto C[(1-x)^4 + 0.5(1-x)^2]$$

This form gives a central part and a leading part to production, with a slope break at $x = 0.3$. To estimate rates in this experiment we have used this form to weight the efficiencies for the different modes presented in section V. The results are shown in Table IV. Because trigger efficiencies are already included, only reconstruction losses will reduce the number of events indicated here. For short-lived states like Λ_c^+ and Ω_c^0 this may be as low as 40% due to impact parameter cuts. For long-lived states it will be $\sim 80\%$.

We assume the following running efficiencies:

16 week run

75 hours per week

60 pulses per hour

20% deadtime and 20 second spill

$A^{0.67}$ dependence (no enhancement) of heavy flavor production

This leads to a data set of 6×10^{10} interactions per running period. In order to convert this to yield of charm states, one must use the x-averaged efficiency and estimate charm cross sections and branching ratios. Table IV gives those results for the charm x distribution indicated earlier and for the cross sections and branching ratio assumptions shown there.

TABLE IV

| Reaction | average | assumed | | number of triggers |
|---|------------|---------|------------------|--------------------|
| | acceptance | BR | σ | |
| $\Lambda_c^+ \rightarrow \Lambda^0 \pi^+$ | 0.28 | .10 | 20 μb | 0.5×10^6 |
| $p K^- \pi^+$ | 0.30 | .05 | | 0.25×10^6 |
| $\Xi_c^+ \rightarrow \Lambda^0 K^- \pi^+ \pi^+$ | 0.28 | .05 | 20 | 0.25×10^6 |
| $\Omega_c^0 \rightarrow \Xi^- \pi^+ K^- \pi^+$ | 0.26 | .10 | 5 | 0.1×10^6 |

From the yields indicated here, it is clear that this apparatus will be a rich source of charm physics. If one were extremely pessimistic and argued that there is no leading term, then for pure $(1-x)^4$ behavior of $d\sigma/dx$, 16% of the cross section lies forward of $x=0.2$. Typical decay modes in SELEX would have 30% detection efficiency, so the yield would still be 80,000 events per run for a state with $\sigma \cdot B = 0.5 \mu\text{b}$. If we were to discover that this condition were true, then the trigger conditions and the Cerenkov tags could be adjusted to increase the average efficiency by another factor of 5 in the next running period. Therefore, the performance of this system is flexible enough to handle

a wide set of possible physics conditions for charm baryon production.

For beauty production we emphasize here the capabilities for studying semileptonic decays. While this mode suffers from the quadratic ambiguity of the neutrino, it is likely to have fewer particles produced and fewer overall neutrals produced than the hadronic modes. Also, its large branching ratio makes it accessible to experiments with interaction rates of 10^5 Hz. As mentioned in section V, the level 3 trigger can identify electron candidates in the TRD and measure their p_t . This selection process can greatly enhance B physics, as is well known. There is very little contamination to the B trigger signal for electron tracks with $p_t > 0.6$ GeV/c. The B efficiency with this cut ranges from .22-.56 as x increases. The issue for SELEX is the size of the B cross section. Bjorken has suggested that the B cross section has leading behavior like charm, but with the leading contribution scaled by the ratio of quark masses. With this form and assuming 10 nb/nucleon beauty production cross section and a 12% semileptonic branching ratio, we expect ~ 120 triggered beauty events per running period. Because these all have the electron fully reconstructed in the VSSD in the trigger level, complete with impact parameter and p_t cut, they should be essentially background-free. This event sample will suffice to establish the level of B production from hyperons and should say something about baryon versus meson contributions and x dependence. If the yield is large enough to warrant further emphasis, we note that the hyperon beam intensity can be increased by a factor of 5 or so; we are nowhere near the intensity limit on the P Center target. In a dedicated run, the trigger can be tuned to electrons, so the extra rate can be handled by limiting the trigger scheme. This rate increase won't endanger the silicon electronics or cause undue radiation damage, since the beam area is large. Thus, there is a reasonable expectation that SELEX can also make a useful contribution to B

physics early in its operation.

VII. DATA ACQUISITION SYSTEM

The trigger discussion has already alluded to the data acquisition structure: data buffer memories for each readout system, followed by extensive computing power to filter events by a factor of 40 after the first level scintillator trigger. This is outlined in fig. 9. We hope to profit from current activity of the Fermilab electronics group, based on work already in progress under the DAWG program. Their proposals are well-matched to our needs. We strongly support this line of development.

The data rates in this apparatus are significant. The average size of 10 kbyte/event is modest. The interaction rate of 50 kHz is modest. However, since 20% of this sample must be carried along through the computational trigger level, the event buffer must be large - 2 Gbyte. Half of this data storage could be in the event processors, the rest in the local memories. The bus rates are also large; we challenge FASTBUS. In order to make the trigger decision we must process 1.2 kb/event. This presents an average data transfer rate of 1.2 Mbyte/sec to the front end bus if one leaves the remaining 90% of the data in the event buffers until events are selected for transfer to tape. Such a system can be built if expanded buffer memory modules (132 Mbyte) are built. The system output is 250 10-kbyte events per second during the 20 second spill, or 5000 events totalling 50 Mbytes. If this is written over the whole spill, then the transfer rate is 1 Mbyte/sec. The new VHS video tape recording systems from 3M and Honeywell have data rates of 3-4 Mbyte/sec and storage capacities of 5 Gbyte/tape. While these are brand-new technologies, they are on the market today. In 1989 the reliability information on these systems will be greatly improved. One can decide if this attractive scheme will really work or if one must resort to multiple output media. These data

rates with multiple 200 kbyte/sec VHS recording systems are now being used at Los Alamos.

The monitor computer does not have to be nearly as sophisticated as the data acquisition processors. We expect that VAXONLINE will be fine. It can sample events from the queue going off to tape. The primary monitoring problem will be to ensure the alignment accuracy. If we are going to make tight online cuts on impact parameter, then we must exploit the large size and angular divergence of the hyperon beam to maintain an ongoing check of all silicon alignments.

VIII. SCHEDULE

There is competition for this physics from proposal P233 at CERN. The group from WA62 plus the Omega spectrometer group now doing WA82 have proposed to build a 300 GeV hyperon beam to work in Omega. While the flux for that beam is roughly a factor of 20 below what one can achieve in the Fermilab beam, the spectrometer is a well-established tool with a significant body of software for extracting physics rapidly. In order to be competitive, P781 cannot give them a significant head start, even though the advantageous duty factor and higher beam energy available at Fermilab give us an intrinsic advantage. Another CERN group has submitted a letter of intent to upgrade the NA14 tagged photon apparatus to make a high rate hyperon facility. Again, the time scale is 1990. Therefore, we must be ready to have a first run in the 1990 fixed target period. This will be an all-charged mode run, to establish cross section levels and verify the triggering scheme. As such it will emphasize the reactions listed in the rate tables. In the following running period, we would expect to develop the apparatus fully and work on modes including π^0 s.

IX. COSTS

The cost estimate given in the letter of intent for SELEX was \$4M. This estimate still holds, as outlined below. The number of different detector elements is given in Table II. To convert this to costs, we have use the following scalings:

| | |
|---|---------------|
| silicon detector planes, PWC planes, drift planes | \$5K/plane |
| silicon analog readout | \$50/channel |
| silicon digital readout (Microplex) | \$ 3/channel |
| PWC readout | \$10/channel |
| drift readout | \$100/channel |

We have assumed that the TRD systems, the downstream silicon detectors covering the deadened region of chambers, the Pb glass, the LAC, and the neutron calorimeter all exist. New construction costs (upstream silicon, drift chambers, PWCs) total \$2.0M. The data acquisition system (fast processors, event memory, 12 FASTBUS crates and supplies), and VHS tape system and host computer totals \$1M. This is the new capital required. PREP electronics needs for fast logic and FASTBUS analog readouts have not yet been included. The value of reclaimed equipment is roughly \$1M, to give the \$4M total.

APPENDIX I

Triggering is the key to achieving the charm event rates sought in this experiment. Because we do not want to bias ourselves toward any one particular decay mode, we have decided to emphasize an impact parameter trigger. This necessarily implies a lot of computation. In order to reduce the load on the processors as much as possible, one would like to use all possible event characteristics to reject background at the earliest possible stage. In SELEX the plan is to use four levels of triggering. These are described in detail

below.

(1) Level 1 Trigger

In this proposal the expected interaction rate is 50kHz. We hope to write events to tape at 250 Hz. The only problem to be solved is how to achieve a factor of 200 reduction in trigger rate without losing any charm events. In the first level, a fast trigger decision is made to indicate the following conditions:

valid beam * interaction * high momentum

The beam composition and rates were discussed earlier. Valid beam will involve the beam scintillators, the beam TRDs, and signals from the beam SSDs. The scintillators and silicon amplifiers will operate at 2 MHz, since the π contamination will count in them as well. The beam TRD signals are available within 100ns to validate the beam particle as a Σ^- . Silicon wafer interaction counters will select interaction events on a beam particle by beam particle basis at a 50kHz rate. Beam deadtime is needed only for the decision time of the interaction counter (50ns). The deadtime should be < 10%. After each interaction, an additional 50ns deadtime is required to decide if the beam particle was a Σ^- , using the beam TRD. This adds negligible deadtime. The final requirement for "high momentum" is imposed by scintillator hodoscopes downstream of the second bending magnet. Three banks of 1cm strips are used to select positive, stiff tracks from the negative incident beam. After these three banks there is a 26m long decay space in which $\Lambda^0 \rightarrow p\pi^-$ decays are selected in a 10 mrad cone around the incident hyperon beam direction. The "high momentum" requirement is:

2 fast positive tracks

OR

1 fast positive track * VEE trigger

These conditions give good triggering efficiency on all the charmed baryon decay modes that we have considered, with one caveat to be discussed later. In fig. 7 one sees the effect of this type of trigger selection on the apparatus acceptance for several specific decay modes of interest. These decay modes involve a variety of final state particles. The uniformly high acceptance indicates that this type of selection will select large x production of charmed baryons in many different modes.

In order to establish exactly how effective this enhancement will be, we have studied the effects of this matrix cut on p -Carbon interactions at 800 GeV taken in the E653 apparatus. These data should have distributions similar to Σ^- Carbon interactions, according to the additive quark model. The s -quark contribution will be lower than the u -quark contribution in proton interactions, so the hyperon multiplicities may be slightly lower than those shown here. To estimate the effects of these matrix cuts, we show in fig. 8 the number and multiplicity distributions in p -Carbon interactions before and after the matrix cut. As you see, imposing a "2 fast wrong-sign tracks" selection reduces the raw interaction rate by a factor of 5. This figure also shows the reduction in track density made by imposing the "high momentum" and "wrong-sign" criterion in the tracking. The mean track density from fig. 8(a) to fig. 8(c) goes down by almost a factor of 3.

The Λ^0 background in the "high momentum" selection can also be estimated from these data plus information from WA62 about the inclusive cross section for $\Sigma^- + Be \rightarrow \Lambda^0 + \text{anything}$. From WA62 data at 135 GeV/c, the probability per interaction of producing a forward Λ^0 is 3% for x bins of 0.3-0.5 and 0.5-0.7 and 4% for $x > 0.7$.²⁴ This background can trigger in two ways. Upstream Λ^0 decays can conspire with background to give "2 fast" matches in the matrix. Downstream decays will give a VEE trigger to combine with a "1 fast" signal

from the matrix. To estimate the suppression of this background by the trigger matrix, we have added a $\Lambda^0 \rightarrow p\pi^-$ decay to the p-Carbon events and reanalyzed them with the trigger requirement that there be 1 wrong-sign fast track in the matrix and a downstream VEE decay to see what fraction of this 10% survive the selection criterion.

For a decay region from 8-34 meters, the fraction of Λ^0 which decay is about 50% for all x from 0.3-1.0. The downstream VEE requirement is based on a multiplicity-jump trigger in the forward 10 mrad cone after 8 meters. In studying the p-Carbon interaction data, we found that less than half of all interactions satisfy the "1 fast wrong-sign" trigger requirement of the matrix. For those interactions which do, the mean charged multiplicity within a 10 mrad cone at 8m is only 0.8 particles per interaction, with an angular spread of 30 mrad or less. As one moves further downstream, even fewer charged particles remain in the 10 mrad cone that contains high momentum Λ^0 . Therefore, a VEE trigger can be made by demanding a multiplicity jump of 2 units between two detectors. The upstream active region subtends 10 mrad. The detector downstream covers a region the size of the upstream area plus an extra annulus needed to cover the angular dispersion of the charged background tracks. The chance of fake multiplicity jump triggers, based on these data, is 3%. Good Λ^0 decays can be lost due to charge jumps of less than 2 if background particles leave the sensitive area. For the data studied this loss is < 2%. The result of these studies is that 16% of the Λ^0 inclusive events will satisfy the "high momentum" trigger. Thus, the total level 1 trigger rate is expected to be 22% of the Σ^- interaction rate, or 11 kHz.

This discussion of "level 1" triggering has not yet dealt with two other important decay modes of charmed baryons: semileptonic modes and modes with neutrons. The semielectronic modes will be triggered by the electron TRD in

level 3. A decay like $\Lambda_c^+ \rightarrow \Lambda^0 e^+ \nu$ will trigger either as "2 fast wrong sign" or "1 fast wrong sign + VEE" for Λ^0 decays upstream of the matrix or after the matrix selection. In either case the scintillator trigger will have selected the candidate. Later processing will check track segments in the TRD for electron candidates. Thus, semileptonic decays are included properly in the trigger.

The neutron decay modes are a different problem. The Cabibbo-unfavored analog of the decay $\Lambda_c^+ \rightarrow \Lambda^0 \pi^+$ is $\Lambda_c^+ \rightarrow n \pi^+$. This will not be selected by the level 1 logic as outlined, although the analogous mode $\Lambda_c^+ \rightarrow \Delta^0 \pi^+$ will be. In order to pick up these neutron modes, one must add another branch to the "high momentum" selection, viz., "single fast wrong sign * neutron". The forward neutron calorimeter covers the necessary solid angle and is fast enough to do this job. From E715 data, one knows that at 300 GeV the neutron calorimeter counting rate per incident Σ^- is very low, essentially that from Σ^- decay, when there is no target. The rate of inelastic neutron production at large x from incident Σ^- is not known, so we cannot estimate this particular tag's sensitivity. In non-kink modes, e.g., $\Lambda_c^+ \rightarrow p \pi^+ \pi^-$, the level 1 trigger works perfectly well for the Cabibbo-unfavored modes.

We conclude that this level 1 trigger scheme will give roughly a factor of 5 rate suppression of the raw interaction without any significant loss of charm events in any decay mode. The purpose of "level 1" selection is to reduce the raw interaction rate to a level that will permit us to reconstruct all the tracks downstream of M2 with a set of very fast processors operating in parallel. Once a track segment is reconstructed, its momentum can be estimated rather accurately from a simple algorithm. The initial matrix trigger selection can be reinforced by the more accurate momentum selection from tracking. We find that half of the p-Carbon events that trigger the

matrix are from high-momentum "right-sign" track pairs that satisfy the matrix conditions. The microprocessor tracking will give a quick additional rejection factor of 2 in the system to be described below as level 2.

(ii) Level 2 Trigger

One of the tenets of the SELEX design is the use of large-x production to reduce the complexity of triggering on charm decays. The level 1 trigger employs event characteristics in the scintillator trigger. Next, we would like to make a fast reconstruction of tracks that meet these trigger requirements. This is done by fast digital processors in "level 2".

In level 2 the aim is to isolate events in which there are "interesting" track candidates - ones which may have come from a heavy flavor decay. Information for tracking is provided by a set of x- and y-PWCs interleaved with the drift chambers after M2. These chambers cover the solid angle defined by the matrix scintillators, approximately 0.5m wide x 0.3m high. Wire spacing is 2mm. With standard readout electronics of the sort that already exists for E761 one can do cluster-finding and locate hits in these chambers to the nearest millimeter. The hits are latched by a valid trigger from level 1 and moved through the event memory into the next available processor to be reconstructed.

The number of "wrong-sign tracks" expected in this region is very modest - 4-5 per interaction. The overall number of tracks may vary up to 15 or so, but many of those are too slow to be interesting. If one reconstructs the slope and intercept of a track at the bend plane of magnet M2, then it is an easy computation to obtain the upstream slope and position at the last VSSD plane, the momentum, and the predicted position of the Cerenkov ring for π , K, or p mass assignments.

Thus, level 2 tracking downstream of M2 allows us to:

- a) filter the level 1 trigger and reject another 50% of the background;
- b) project tracks downstream into the RICH and predict the photon hit pattern in the RICH photomultiplier matrix, for online particle identification in the level 3 trigger;
- c) project tracks upstream to predict slopes and positions in the vertex silicon detectors to begin impact parameter calculations for the level 3 trigger.

How well does all this work? This algorithm was applied to data from 800 GeV p-Carbon interactions which survived the matrix selection in the level 1 trigger. The relevant characteristics of these events are shown in fig. 8. The mean multiplicity in ± 120 mrad in the vertex region is 11 ± 5 tracks. After M2 the mean multiplicity is 6.3 ± 2.3 . Of these, 4.3 ± 1.5 fall in the tracking window and are reconstructed by the algorithm. This refinement of the track set is made chiefly by imposing the "wrong-sign" requirement in the tracking algorithm. These are the track candidates most likely to have come from charm decays. Also shown in fig. 10 are the algorithm statistics showing the number of segments found compared with the number of real tracks to be found. These data assume 98% per plane chamber efficiency for single-wire counting rates in the beam region of 500 kHz or less. From previous experience with chambers of this size in this kind of environment, we should be able to do at least this well.

(iii) Level 3 Trigger

In order to compute the impact parameter of each downstream track with full vertex detector resolution, one must do a complete track reconstruction in the silicon detectors. While this is in principle time-consuming for the usual 11

tracks/interaction, we have predicted the slope and intercept point of the downstream tracks at the last silicon plane in level 2. This reduces the scope of the tracking problem immensely and makes the calculation of the impact parameter for each downstream track segment a tractable online computing problem.

Of course, the downstream information is helpful only if the extrapolation is good. To study that, we have taken the p-Carbon track segments found by the level 2 trigger computation and projected them back upstream. The resolution is limited by the approximation of simple bend planes for the two magnets and by the resolution of the chambers. All the tracks in which we are interested are small angle, high momentum tracks. They tend to go through the central field region and have minimal fringe field vertical bending. Therefore, for this set of tracks the simple bend plane approximation is good to at least 1%. Since we are after 5% effects, this is not the limiting effect; resolution is determined by PWC wire spacing.

The match between predicted track position and slope is good to ± 1 mm and ± 1.5 mrad for tracks at angles less than 10 mrad from the beam direction and ± 2 mm and ± 2 mrad for tracks out to 30 mrad. It takes 2 ms of 8600 time to find not only the upstream matches to the downstream segments but also to pick up, on the average, another 4 tracks which fall in the ± 1 mm window around the expected upstream track position. These tracks are reconstructed with the full resolution of the vertex silicon detector, i.e., $8\mu\text{m}$ impact parameter resolution and $20\ \mu\text{rad}$ angular resolution.

The next stage of the level 3 computation entails figuring which target foil was struck, so that the impact parameter can be estimated using the center of that target foil. Taking a 1mm maximum target thickness, we obtain impact parameter resolution of $\sigma_b = t\theta/2$ for foil thickness t , track angle θ . For a

typical charm track $\theta = 5$ mrad, so $\delta_b = \pm 2.5 \mu\text{m}$. The impact parameter uncertainty is influenced almost equally by the beam resolution ($3 \mu\text{m}$), the upstream plane's spatial resolution ($3 \mu\text{m}$), and the target thickness effect ($\sim 3 \mu\text{m}$). Thus, $\delta_b < 6 \mu\text{m}$, while the total impact parameter $b > 20 \mu\text{m}$ in 60% of Λ_c^+ decays. This is the basis for the trigger.

From the study of p-Carbon events one sees that in all the triggers that survive the level 2 momentum cut there is at least one reconstructed track with an angle of > 3 mrad. This angle is large enough that even including track errors, the intersection of this one track with the beam trajectory determines unambiguously in which target foil the interaction took place. In the case of kink decays, there can be cases in which the charm secondary and the one reconstructed primary track point to different beam foils. This is not a problem. Such cases automatically give an impact parameter to one or the other track and will be passed on to the next processing stage for full reconstruction in the vertex SSDs. The rate of such events is a fraction of the charm rate, so the load on the processing system is minimal. The distribution of upstream track angles for reconstructed level 2 tracks is also shown in fig. 10(c).

The aims of level 3 triggering are:

- a) reconstruct the upstream track segments corresponding to the tracks found in the downstream PWCs in level 2;
- b) locate the target foil in which the primary interaction took place, using the beam track and these reconstructed VSSD tracks. In case of ambiguity, pass the candidate along to level 4.

(iv) level 3a

The discussion so far has been aimed at triggers for general heavy flavor decays. There is other physics for which SELEX is appropriate. In the letter of intent we observed that the exotic U meson suggested by the WA62 data should be verified. This meson will not exhibit a nonzero impact parameter, since it decays strongly. However, it has a characteristic particle composition which allows for a RICH trigger. One can use the track segments found in level 2 to point into the RICH and predict the ring radii from lookup tables for π , K, or p mass assignments. The lookup table would define which pixels in the RICH should be lit for any of the three possibilities, and a simple integer matching routine would suffice to give a trigger-level mass tag to each particle. In this case, level 4a would trigger on "quantum number tags" - double strange mesons, strange wrong-charge baryons, etc. The U meson tag in WA62 was $\Lambda^0 \bar{p} + X$, for example. For studies of high mass Ω states, double strangeness tags may be helpful, or $\Lambda^0 K^-$ states are interesting. This kind of selection is easy to implement with our trigger scheme; it is completely software controlled.

In addition, the more unusual charmed baryon states may profit from having the RICH included in the trigger. Σ_c and Ω_c decays will generate multiple-strange particle final states. Therefore, triggers like

$$K^- * VEE * \text{"single fast"} \quad \text{or}$$

$$2K^- * \text{"single fast"}$$

may help to select these decay modes. Such triggers are available at level 3.

(v) level 4

The last level of the impact parameter trigger refines the level 3 information on the primary vertex position by reconstructing 3 dimensional tracks in the VSSD. Using the selected target foil center and the beam track along with the VSSD tracks, a full 3d least squares fit is to be done. The

fitted parameters and the vertex position are used to look for impact parameters exceeding 20 μ m. The aim of this pass is to make a rate reduction by a factor of 20. At that rate we can write to VHS tape with most charm still in the sample.

LIST OF REFERENCES

- 1 S.F.Biagi, et al. Phys Lett 122B, 455(1983); Phys. Lett. 150B, 230(1985)
- 2 Split-Field Magnet Collaboration, seminar at CERN, May, 1987 and T. Nakada, SIN, private communication
- 3 P. Coteus, et al., Phys. Rev. Lett. 59, 1530(1987)
- 4 S. Barlag, et al., Phys Lett. 184B, 283(1987)
- 5 H. Becker, et al., Phys. Lett. 184, 277(1987)
- 6 M. Dreisberg, et al., Fermilab preprint
Argus collaboration, submission to Berkeley Conference, 1986 and K. Edwards, private communication
- 7 B. Guberina, et al., Z. Physik C33, 297(1986)
- 8 S.F.Biagi, et al., Z. Physik C28, 175(1985)
- 9 The only reported excited baryon is a Σ_c^* reported by Argus. K. Edwards, private communication.
- 10 Mark III collaboration, SLAC PUB 4291, June, 1987
- 11 M. Aguilar-Benitez, et al., Phys. Lett. 189B, 254(1987)
- 12 In E400, for example, the system of 3 threshold Cerenkov counters gave unambiguous K^+K^- tags only for D mesons in the x range 0.07-0.15.
- 13 R.J.Apsimon, et al., Nucl. Instr. and Meth. A248, 76(1986)
- 14 S. Shapiro, talk at the LBL Workshop on Physics at the SSC, Berkeley 1987
- 15 M.K. Gaillard, B. Lee, and J. Rosner, Rev. Mod. Phys. 47, 277(1975)

- 16 M. Wirbel, B. Stech, and M. Bauer, Z. Physik C29, 637(1985)
B. Grinstein, M.B. Wise, and N. Isgur, Phys. Rev. Lett. 56, 298(1986)
- 17 D. Ebert and W. Kallies, Z. Physik C29, 643(1985)
- 18 E. Belau, et al., Nucl. Instr. and Meth. A214, 253(1985)
M. Caccia, et al., CERN-EP/87-81
- 19 J.E. Arens and J. Garrett Jernigan, LBL Space Sciences Lab, private commun.
- 20 R. Ammar, et al., Phys Lett. 183, 110(1987)
- 21 M. Aguilar-Benitez, et al., Phys Lett. 189, 476(1987)
- 22 L. Montanet, private commun.
- 23 LAMPF MEGA experiment; P. Cooper, private commun.
- 24 H.-W. Siebert, unpublished data from WA62

LIST OF FIGURES

- FIGURE 1 x distributions for Ξ_c^+ from (a) WA 62, 135 GeV/c Σ^- - Be collisions; and (b) E 400, 600 GeV nA interactions
- FIGURE 2 Valence quark diagrams illustrating similarities and differences in charm baryon production at large x by Σ^- , p, and n beams
- FIGURE 3 Dalitz plots for $\Xi_c^+ \rightarrow \Sigma^+(1385) + K^0(890)$ (a) from WA 62 data, and (b) Monte Carlo of pure resonance final state
- FIGURE 4 SELEX Spectrometer layout in P Center
- FIGURE 5 Beam TRD separation curves for 600 GeV beam, equal Σ^- and π^- flux
- FIGURE 6 (a) Impact parameter trigger layout in WA82 (b) Impact parameter resolution for tracks associated with primary vertex in WA82.
- FIGURE 7 Geometric acceptance and trigger matrix efficiency versus x for
(a) $\Lambda_c^+ \rightarrow \Lambda^0 \pi^+$ (b) $\Lambda_c^+ \rightarrow p K^- \pi^+$
(c) $\Xi_c^+ \rightarrow \Lambda^0 K^- \pi^+ \pi^+$ (d) $\Omega_c^0 \rightarrow \Sigma^- K^- \pi^+ \pi^+$
- FIGURE 8 Distributions of tracks per event from 800 GeV p-Carbon interactions

with interaction trigger. Events selected to come from target.

(a) tracks/event in VSSD region (b) tracks/event-after M2

(c) tracks/event in trigger region, emphasizing negative tracks

Cross-hatched histograms are for events which pass trigger matrix cut

FIGURE 9

Schematic of Data Acquisition Architecture. Only one

FASTBUS segment is allowed for front end buffers.

Processors have separate input and output busses.

FIGURE 10

PWC tracking test results. (a) number of segments found versus

number of real tracks after M2 (b) number of VSSD tracks

reconstructed versus number of segments, showing the

increase in average number of segments upstream.

(c) distribution of x slopes for segments reconstructed in VSSDs

Track angles exceeding 2 mrad are common. Angles of 2 mrad

or larger define in which target foil the primary interaction

occurred, as discussed in Appendix I.

WA62 $d\sigma/dx$ vs x

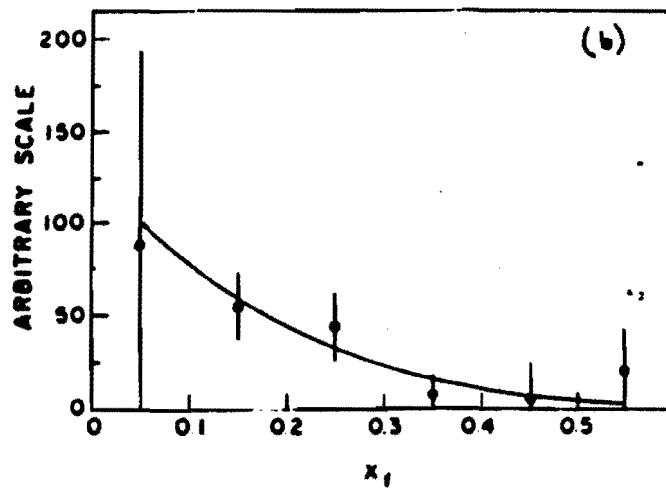
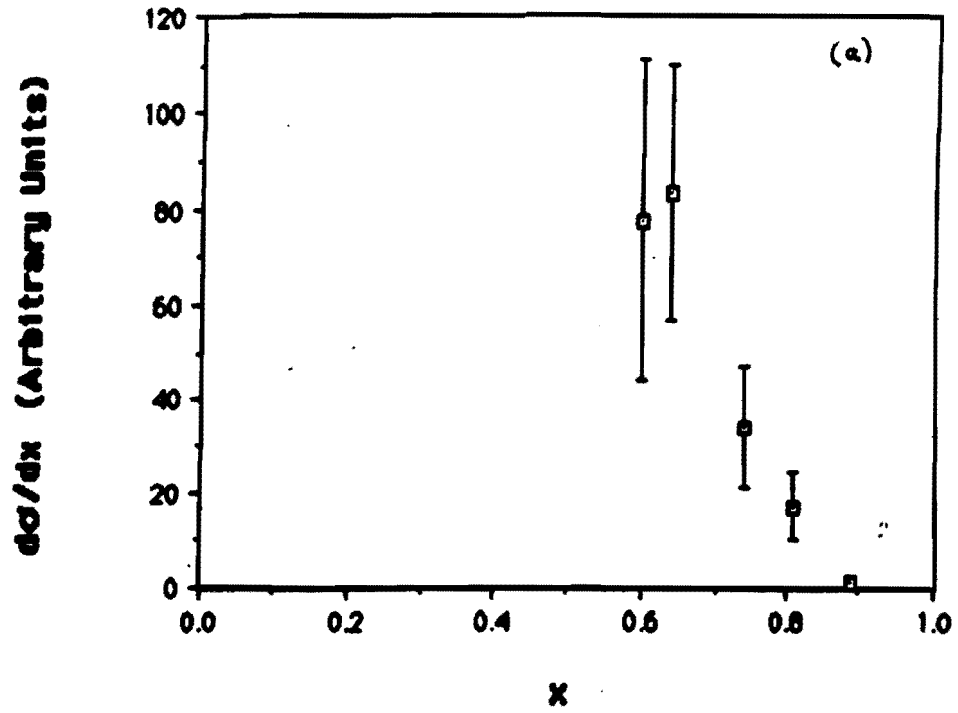


Figure 1

x Distributions for Ξ_c^+ from
(a) WA 62, 135 GeV/c Σ^- Be collisions
(b) E400, 600 GeV nA interactions

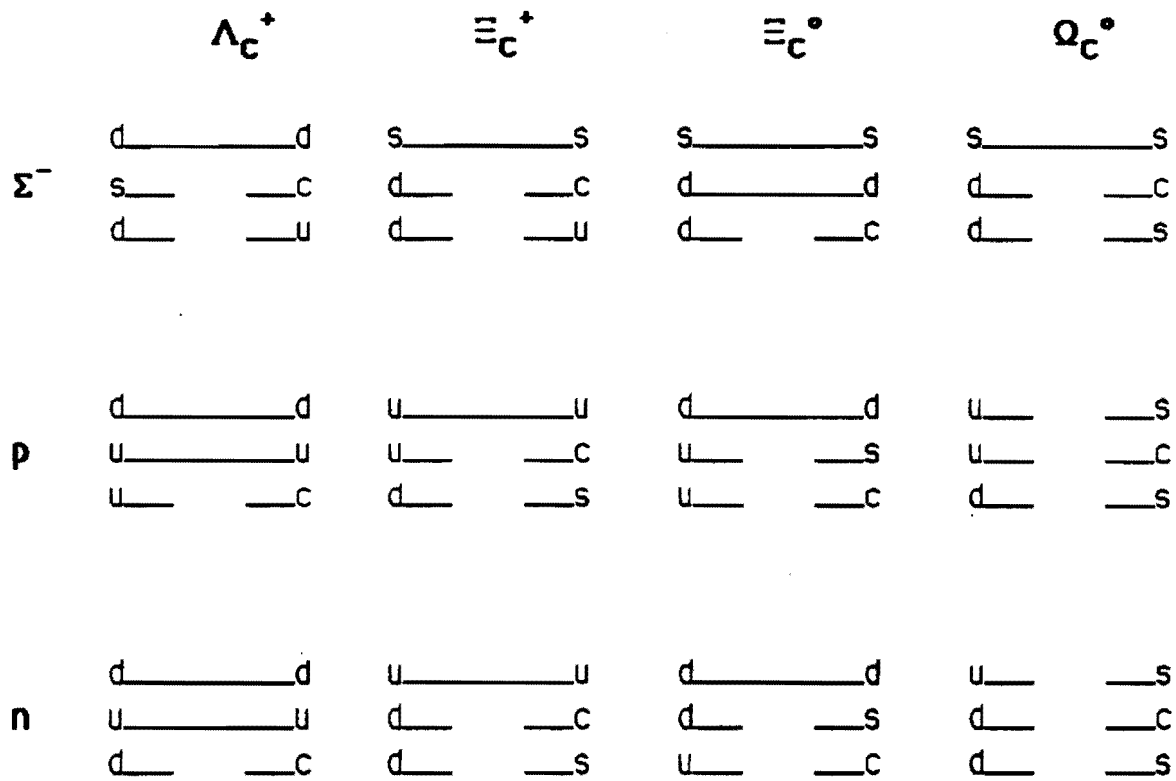


Figure 2

**Naive Valence Quark Diagrams For Charm Baryon
Production From Baryons**

NO SCALE

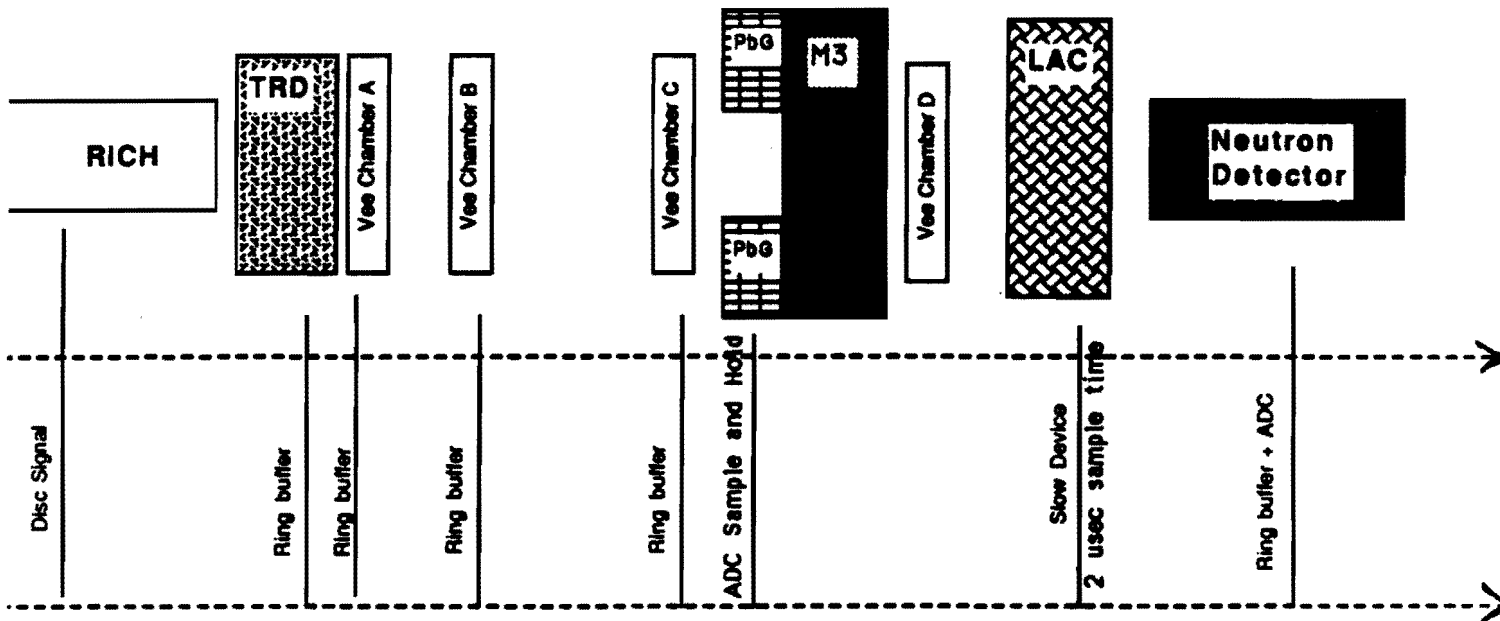
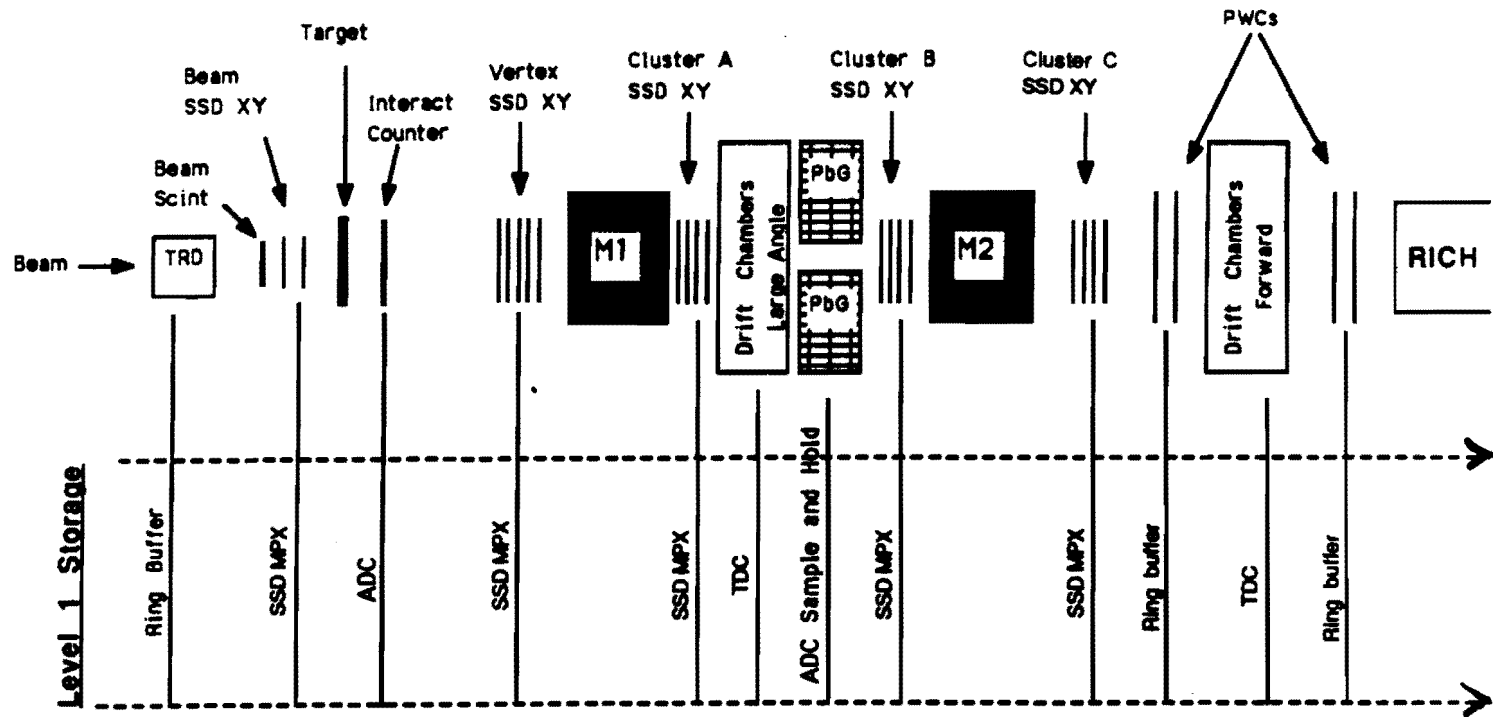


Figure 4

SELEX Spectrometer Layout
See Table II for dimensions

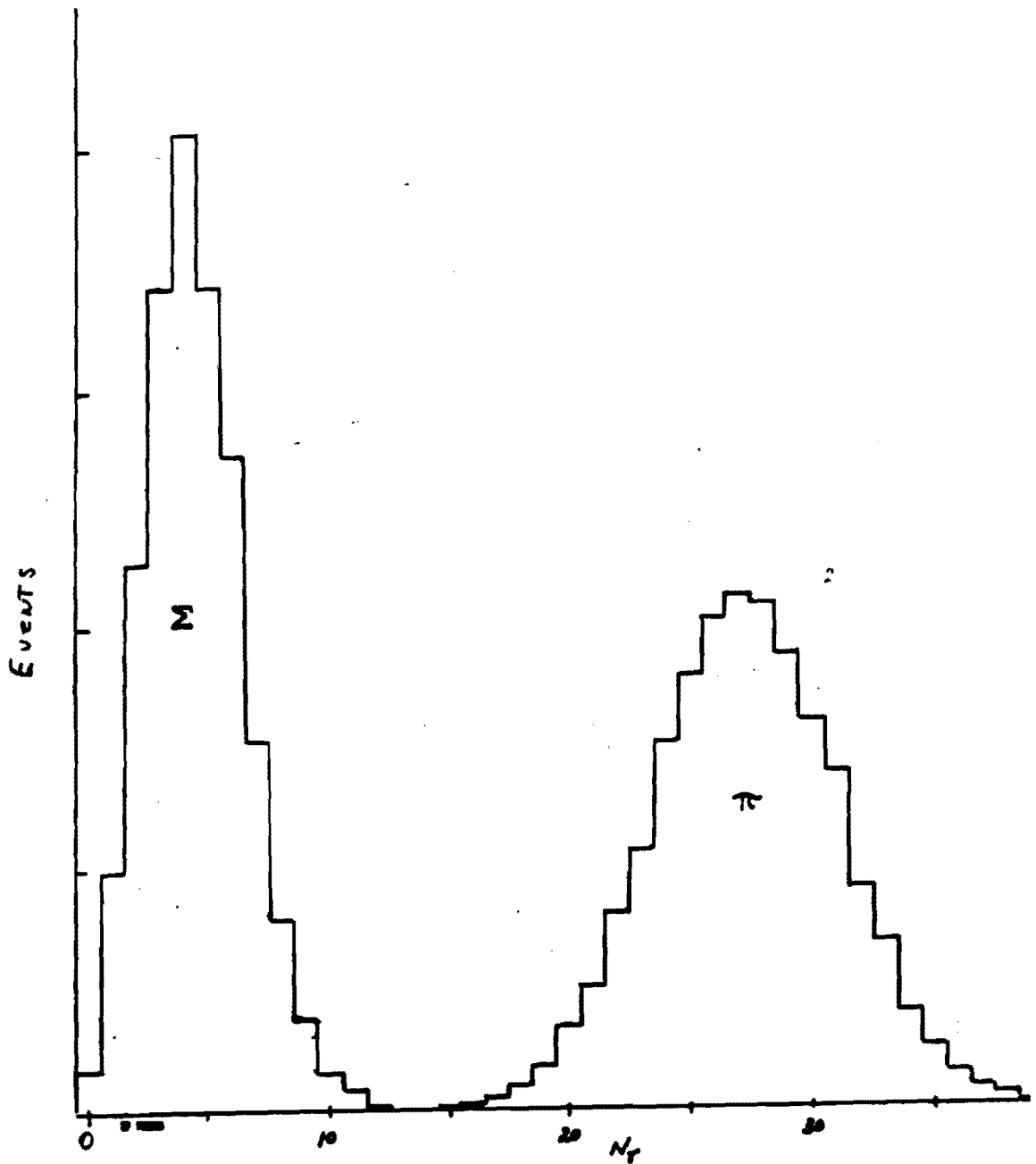


Figure 5

TRD Response to 600 GeV/c negative beam

60 Planes, 20 Modules
6 KeV γ Threshold (70% Xe)
17 μ m CH₂ Radiator Foils
100 ns collection time

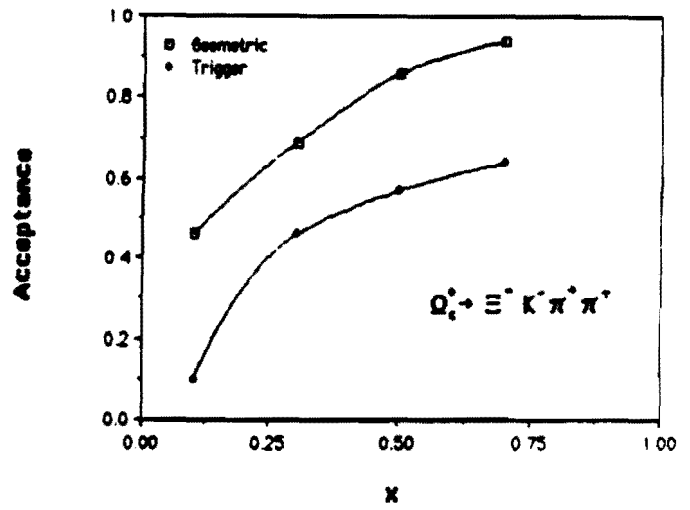
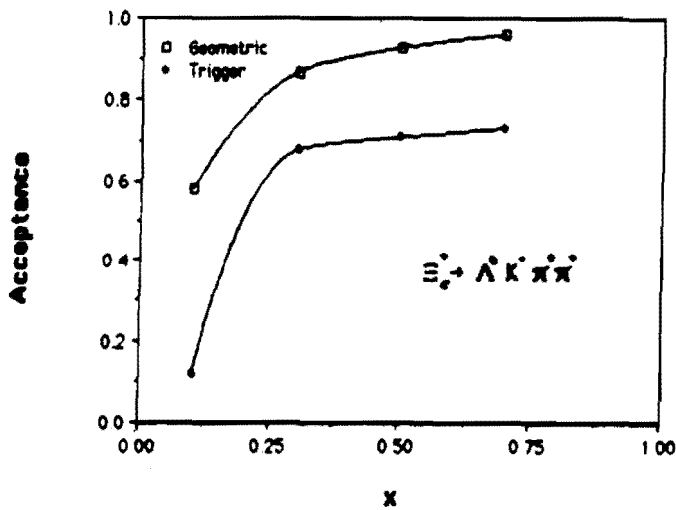
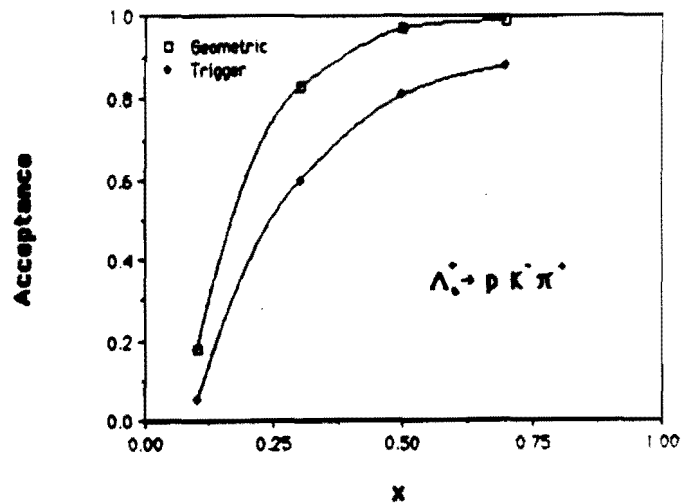
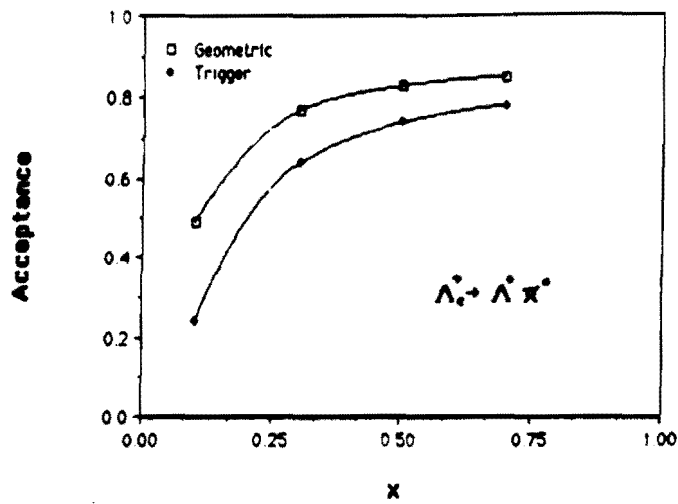


Figure 7

Geometric Acceptance and Trigger Matrix Efficiency Versus x for

$$\Lambda_c^+ \rightarrow \Lambda^0 \pi^0$$

$$\Lambda_c^+ \rightarrow \rho K^- \pi^+$$

$$\Xi_c^+ \rightarrow \Lambda^0 K^- \pi^+ \pi^+$$

$$\Omega_c^0 \rightarrow \Xi^- K^- \pi^+ \pi^+$$

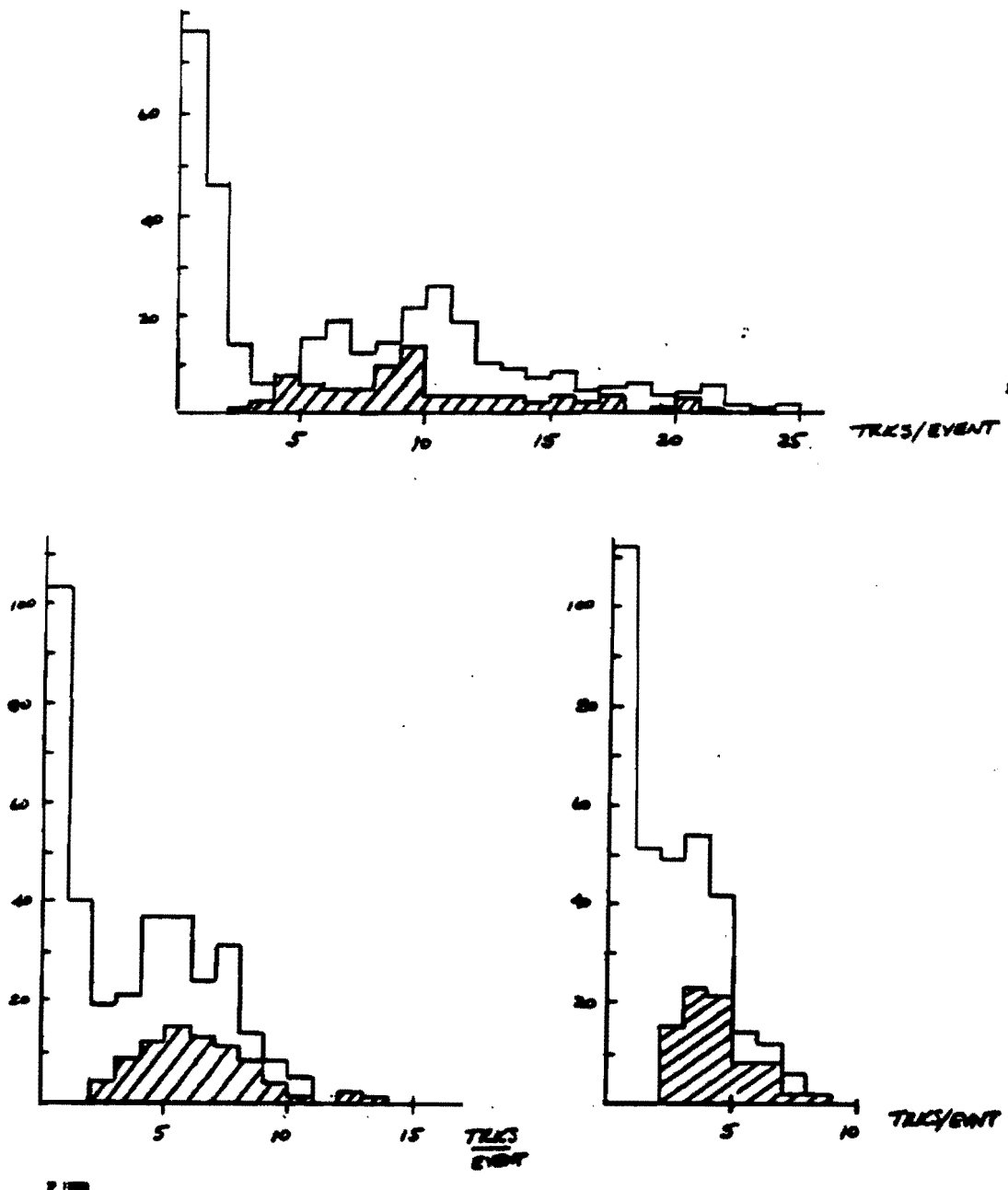


Figure 8

Number of tracks per event distribution for 800 GeV

p-Carbon interactions in

(a) in VSSD

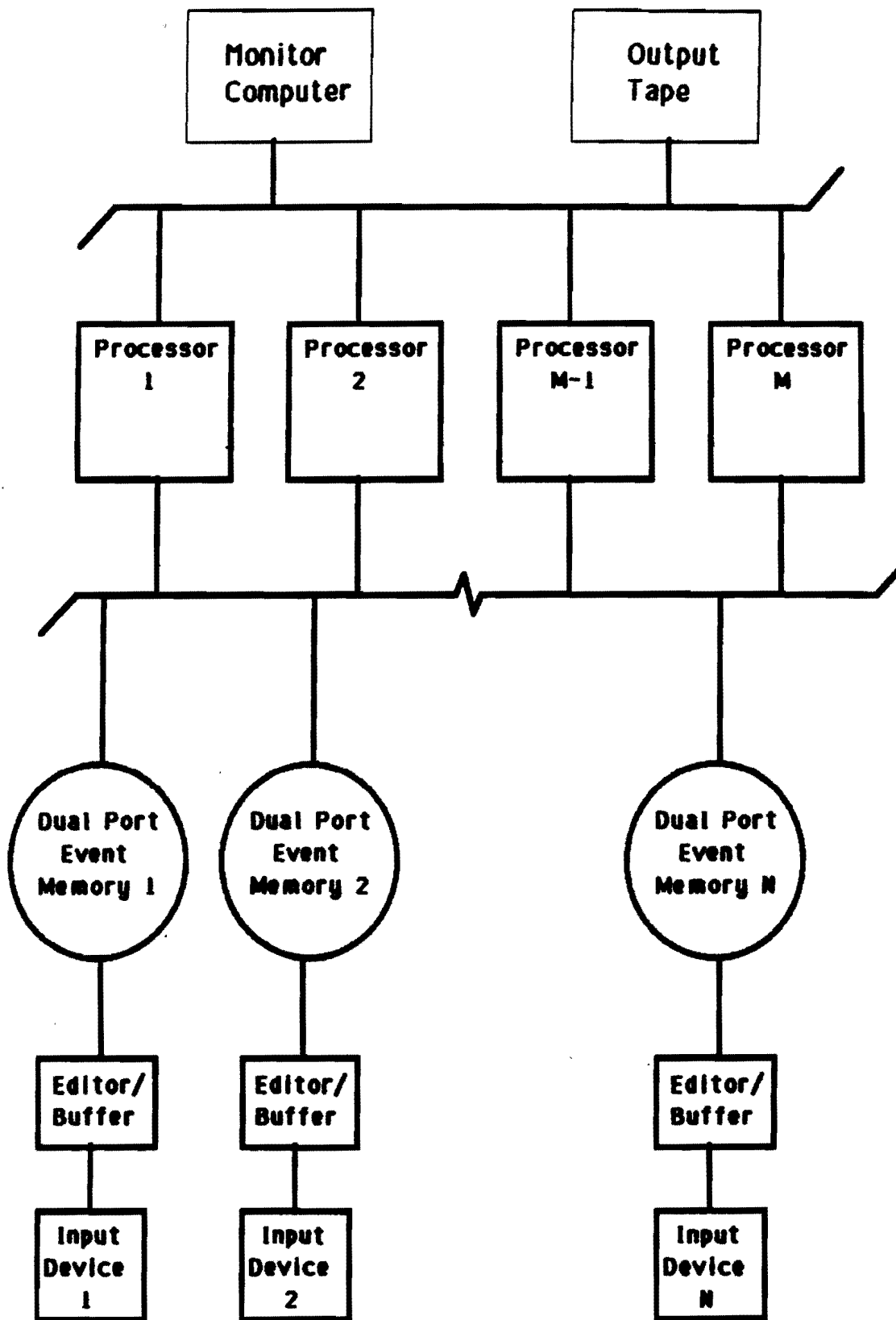
(b) after M2

(c) in trigger region

Cross hatched histograms are events which pass trigger matrix cut

Figure 9

Schematic Data Acquisition Architecture



PWC/VSSD TRACKING STATISTICS FOR 25 EVENTS SAMPLED

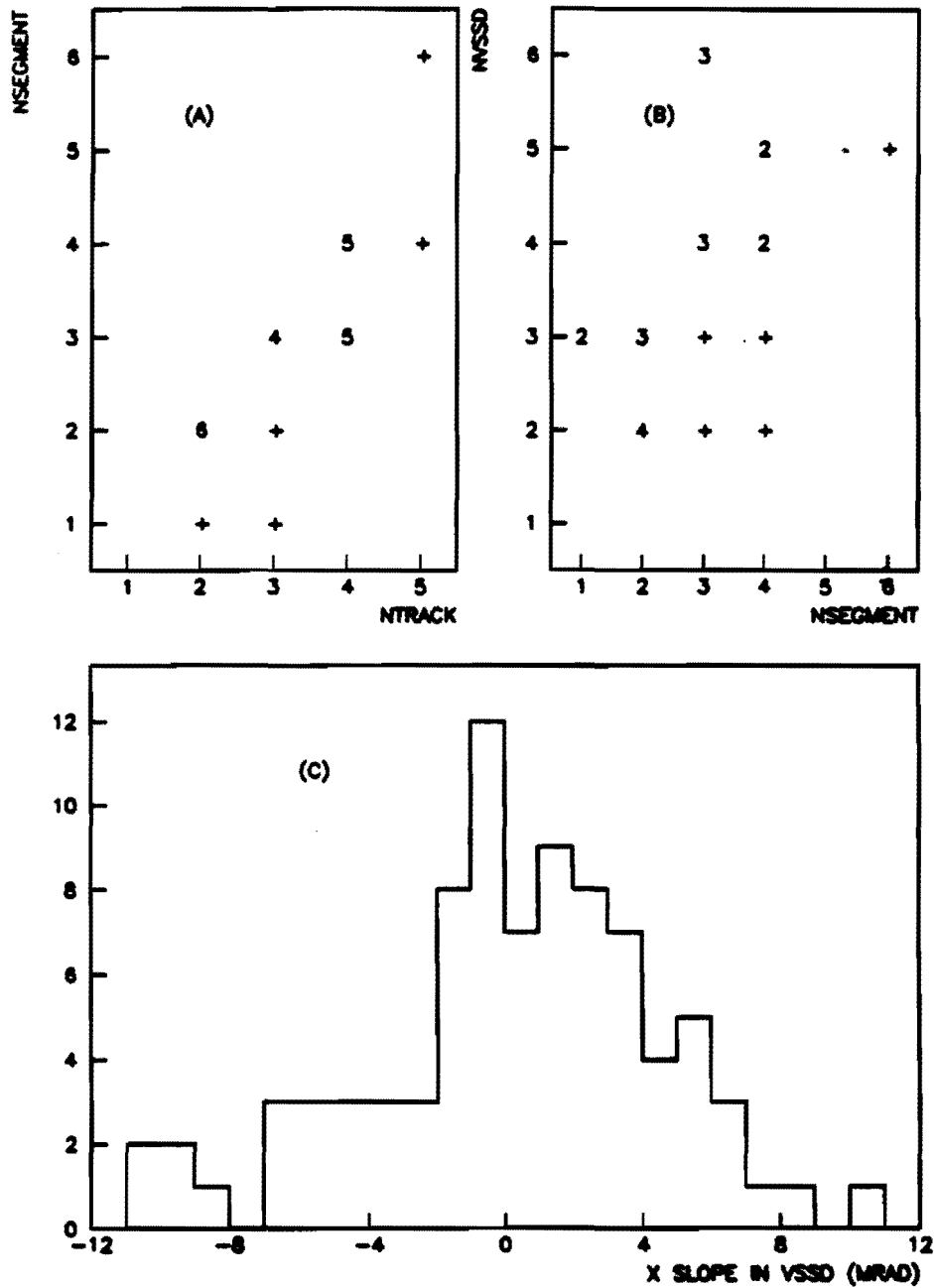


Figure 10

PWC Tracking Statistics

- (a) number of segments found versus number of real tracks in trigger region
- (b) number of VSSD tracks reconstructed versus number of segments found downstream
- (c) distribution of x slopes for segments reconstructed in VSSDs

| Detector | Z position | Active Area (full) | | Pitch cm | Channels | Channels | Bytes/ | Active Channels | | Bytes/Event | | Bytes Sub Total | |
|------------------------|---|--------------------|-------|--|----------|-----------|---------|-----------------|-----|-------------|-----|-----------------|-----|
| | m | X cm | Y cm | | | Sub total | Channel | Average | Max | Average | Max | Average | Max |
| Channel Exit | -3.140 | 0.40 | 0.80 | Exit apertures of Channel, beam divergence is about 1 mrad in each plane | | | | | | | | | |
| Beam TRD | Data in 1 byte: 3 bits for address, rest for number of clusters | | | | | | | | | | | | |
| Beam TRD 1 | -2.890 | 1.00 | 1.00 | | 1 | | 1 | 1 | 1 | 1 | 1 | | |
| Beam TRD 2 | -2.640 | 1.00 | 1.00 | | 1 | | 1 | 1 | 1 | 1 | 1 | | |
| Beam TRD 3 | -2.390 | 1.00 | 1.00 | | 1 | | 1 | 1 | 1 | 1 | 1 | | |
| Beam TRD 4 | -2.140 | 1.00 | 1.00 | | 1 | | 1 | 1 | 1 | 1 | 1 | | |
| Beam TRD 5 | -1.890 | 1.00 | 1.00 | | 1 | | 1 | 1 | 1 | 1 | 1 | | |
| Beam TRD 6 | -1.640 | 1.00 | 1.00 | | 1 | | 1 | 1 | 1 | 1 | 1 | | |
| Beam TRD 7 | -1.390 | 1.00 | 1.00 | | 1 | 7 | 1 | 1 | 1 | 1 | 1 | 7 | 7 |
| Beam SSD | Data in 2 bytes: 2 bits for plane, 2 bits for chip, 7 for strip | | | | | | | | | | | | |
| Beam SSD X1 | -1.140 | 0.50 | 1.00 | 0.0020 | 256 | | 2 | 2 | 5 | 4 | 10 | | |
| Beam SSD Y1 | -1.130 | 0.50 | 1.00 | 0.0020 | 512 | | 2 | 2 | 5 | 4 | 10 | | |
| Beam SSD U1 | -1.120 | 0.50 | 1.00 | 0.0020 | 512 | | 2 | 2 | 5 | 4 | 10 | | |
| Beam SSD X2 | -0.120 | 0.50 | 1.00 | 0.0020 | 256 | | 2 | 2 | 5 | 4 | 10 | | |
| Beam SSD Y2 | -0.110 | 0.50 | 1.00 | 0.0020 | 512 | | 2 | 2 | 5 | 4 | 10 | | |
| Beam SSD U2 | -0.100 | 0.50 | 1.00 | 0.0020 | 512 | 2560 | 2 | 2 | 5 | 4 | 10 | 24 | 60 |
| Target | 0.000 | 0.50 | 1.00 | The target might be a set of 10-1.0 mm foils separated by 1.0 mm | | | | | | | | | |
| Silicon Pad Det | Data in 3 bytes: 2 bytes for address, one for ADC, Each has 256x256 pads, 30 um in size | | | | | | | | | | | | |
| Silicon Pad 1 | 0.010 | 0.01 | 0.01 | 0.0030 | 65536 | | 3 | 25 | 50 | 75 | 150 | | |
| Silicon Pad 2 | 0.020 | 0.01 | 0.01 | 0.0030 | 65536 | 131072 | 3 | 25 | 50 | 75 | 150 | 150 | 300 |
| Vertex SSD | Subtends \approx 0.15 radians in each plane | | | | | | | | | | | | |
| | Data in 3 bytes: 6 bits for plane, 4 bits for chip, 7 for strip, 6 bits for flash ADC | | | | | | | | | | | | |
| Vertex SSD X1 | 0.070 | 2.60 | 3.10 | 0.0020 | 1408 | | 3 | 20 | 40 | 60 | 120 | | |
| Vertex SSD Y1 | 0.090 | 3.20 | 3.70 | 0.0020 | 1920 | | 3 | 20 | 40 | 60 | 120 | | |
| Vertex SSD U1 | 0.110 | 3.80 | 4.30 | 0.0020 | 2944 | | 3 | 20 | 40 | 60 | 120 | | |
| Vertex SSD V1 | 0.130 | 4.40 | 4.90 | 0.0020 | 3328 | | 3 | 20 | 40 | 60 | 120 | | |
| Vertex SSD X2 | 0.150 | 5.00 | 5.50 | 0.0020 | 2560 | | 3 | 20 | 40 | 60 | 120 | | |
| Vertex SSD Y2 | 0.170 | 5.60 | 6.10 | 0.0020 | 3072 | | 3 | 20 | 40 | 60 | 120 | | |
| Vertex SSD U2 | 0.190 | 6.20 | 6.70 | 0.0020 | 4608 | | 3 | 20 | 40 | 60 | 120 | | |
| Vertex SSD V2 | 0.210 | 6.80 | 7.30 | 0.0020 | 4992 | | 3 | 20 | 40 | 60 | 120 | | |
| Vertex SSD X3 | 0.230 | 7.40 | 7.90 | 0.0020 | 3712 | | 3 | 20 | 40 | 60 | 120 | | |
| Vertex SSD Y3 | 0.250 | 8.00 | 8.50 | 0.0020 | 4352 | | 3 | 20 | 40 | 60 | 120 | | |
| Vertex SSD U3 | 0.270 | 8.60 | 9.10 | 0.0020 | 6272 | | 3 | 20 | 40 | 60 | 120 | | |
| Vertex SSD V3 | 0.290 | 9.20 | 9.70 | 0.0020 | 6784 | | 3 | 20 | 40 | 60 | 120 | | |
| Vertex SSD X4 | 0.310 | 9.80 | 10.30 | 0.0050 | 2048 | | 3 | 20 | 40 | 60 | 120 | | |
| Vertex SSD Y4 | 0.330 | 10.40 | 10.90 | 0.0050 | 2304 | | 3 | 20 | 40 | 60 | 120 | | |
| Vertex SSD U4 | 0.350 | 11.00 | 11.50 | 0.0050 | 3200 | | 3 | 20 | 40 | 60 | 120 | | |
| Vertex SSD V4 | 0.370 | 11.60 | 12.10 | 0.0050 | 3456 | | 3 | 20 | 40 | 60 | 120 | | |

| Detector | Z position | Active Area (full) | | Pitch | Channels | Channels | Bytes/ | Active Channels | | Bytes/Event | | Bytes Sub Total | |
|-----------------------|------------|--------------------|--------|---|----------|-----------|---------|-----------------|-----|-------------|-----|-----------------|------|
| | m | X cm | Y cm | cm | | Sub total | Channel | Average | Max | Average | Max | Average | Max |
| Vertex SSD X5 | 0.390 | 12.20 | 12.70 | 0.0050 | 2560 | | 3 | 20 | 40 | 60 | 120 | | |
| Vertex SSD Y5 | 0.410 | 12.80 | 13.30 | 0.0050 | 2688 | | 3 | 20 | 40 | 60 | 120 | | |
| Vertex SSD U5 | 0.430 | 13.40 | 13.90 | 0.0050 | 3968 | | 3 | 20 | 40 | 60 | 120 | | |
| Vertex SSD V5 | 0.450 | 14.00 | 14.50 | 0.0050 | 4096 | 70272 | 3 | 20 | 40 | 60 | 120 | 1200 | 2400 |
| Start Magnet 1 | 0.950 | 40.00 | 25.00 | B=13 kG, Pt=350 MeV/c, Should be .6-1.0 m long, LOOK UP LIST | | | | | | | | | |
| End Magnet 1 | 1.850 | | | | | | | | | | | | |
| Cluster A SSD | | | | Data in 3 bytes: 3 bits for plane, 5 bits for chip, 7 for strip | | | | | | | | | |
| Cluster A SSD X1 | 2.350 | 5.00 | 5.00 | 0.0050 | 1000 | | 3 | 15 | 25 | 45 | 75 | | |
| Cluster A SSD Y1 | 2.365 | 5.00 | 5.00 | 0.0050 | 1000 | | 3 | 15 | 25 | 45 | 75 | | |
| Cluster A SSD U1 | 2.380 | 5.00 | 5.00 | 0.0050 | 1000 | | 3 | 15 | 25 | 45 | 75 | | |
| Cluster A SSD V1 | 2.395 | 5.00 | 5.00 | 0.0050 | 1000 | 4000 | 3 | 15 | 25 | 45 | 75 | 180 | 300 |
| DC Large Angle | | | | Vector Chambers with 5 sense wires per cell | | | | | | | | | |
| | | | | Data in 21 bytes: 5 bits for plane, 2- 2 byte TDC (beg and end) each hit time in 5 sense wires | | | | | | | | | |
| Drift Cham X1 | 2.645 | 100.00 | 100.00 | 2.00 | 50 | | 21 | 20 | 40 | 420 | 840 | | |
| Drift Cham U1 | 2.695 | 100.00 | 100.00 | 2.00 | 50 | | 21 | 20 | 40 | 420 | 840 | | |
| Drift Cham V1 | 2.745 | 100.00 | 100.00 | 2.00 | 50 | | 21 | 20 | 40 | 420 | 840 | | |
| Drift Cham X2 | 2.795 | 100.00 | 100.00 | 2.00 | 50 | | 21 | 20 | 40 | 420 | 840 | | |
| Drift Cham U2 | 2.845 | 100.00 | 100.00 | 2.00 | 50 | | 21 | 20 | 40 | 420 | 840 | | |
| Drift Cham V2 | 2.895 | 100.00 | 100.00 | 2.00 | 50 | | 21 | 20 | 40 | 420 | 840 | | |
| Drift Cham X3 | 2.945 | 100.00 | 100.00 | 2.00 | 50 | | 21 | 20 | 40 | 420 | 840 | | |
| Drift Cham U3 | 2.995 | 100.00 | 100.00 | 2.00 | 50 | | 21 | 20 | 40 | 420 | 840 | | |
| Drift Cham V3 | 3.045 | 100.00 | 100.00 | 2.00 | 50 | | 21 | 20 | 40 | 420 | 840 | | |
| Drift Cham X4 | 3.095 | 100.00 | 100.00 | 2.00 | 50 | 500 | 21 | 20 | 40 | 420 | 840 | 4200 | 8400 |
| Pb6 Upstream | | | | Data in 4 bytes: 2 bytes for block address, 2 for value | | | | | | | | | |
| Pb6 Upstream | 3.195 | 100.00 | 100.00 | 4.00 | 720 | 720 | 4 | 20 | 40 | 80 | 160 | 80 | 160 |
| Cluster B SSD | | | | Data in 3 bytes: 3 bits for plane, 5 bits for chip, 7 for strip | | | | | | | | | |
| Cluster B SSD X1 | 4.195 | 5.00 | 5.00 | 0.0050 | 1000 | | 3 | 15 | 25 | 45 | 75 | | |
| Cluster B SSD Y1 | 4.210 | 5.00 | 5.00 | 0.0050 | 1000 | | 3 | 15 | 25 | 45 | 75 | | |
| Cluster B SSD U1 | 4.225 | 5.00 | 5.00 | 0.0050 | 1000 | | 3 | 15 | 25 | 45 | 75 | | |
| Cluster B SSD V1 | 4.240 | 5.00 | 5.00 | 0.0050 | 1000 | 4000 | 3 | 15 | 25 | 45 | 75 | 180 | 300 |
| Start Magnet 2 | 4.740 | 60.96 | 25.4 | Magnet is BM109 opened up to 10 inch gap and 15 kG, Pt=450 MeV/c | | | | | | | | | |
| End Magnet 2 | 6.740 | 60.96 | 25.4 | This gives a vertical acceptance of ± 19 mrad, ± 46 horizontal Do we want to put in second BM109? | | | | | | | | | |
| Cluster C SSD | | | | Data in 3 bytes: 3 bits for plane, 5 bits for chip, 7 for strip | | | | | | | | | |
| Cluster C SSD X1 | 7.240 | 5.00 | 5.00 | 0.0050 | 1000 | | 3 | 15 | 25 | 45 | 75 | | |
| Cluster C SSD Y1 | 7.255 | 5.00 | 5.00 | 0.0050 | 1000 | | 3 | 15 | 25 | 45 | 75 | | |
| Cluster C SSD U1 | 7.270 | 5.00 | 5.00 | 0.0050 | 1000 | | 3 | 15 | 25 | 45 | 75 | | |
| Cluster C SSD V1 | 7.285 | 5.00 | 5.00 | 0.0050 | 1000 | 4000 | 3 | 15 | 25 | 45 | 75 | 180 | 300 |
| PWCs | | | | These chambers are for use with fast processors. We intersperse Forward Drift Chambers | | | | | | | | | |

| Detector | Z position | Active Area (full) | | Pitch | Channels | Channels | Bytes/ | Active Channels | | Bytes/Event | | Bytes | Sub Total |
|----------------------|------------|--------------------|--------|--|----------|-----------|---------|-----------------|-----|-------------|-----|---------|-----------|
| | m | X cm | Y cm | cm | | Sub total | Channel | Average | Max | Average | Max | Average | Max |
| | | | | Data is in 3 bytes | | | | | | | | | |
| PWC X1 | 7.785 | 100.00 | 50.00 | 0.2000 | 500 | | 3 | 5 | 10 | 15 | 30 | | |
| PWC Y1 | 7.885 | 100.00 | 50.00 | 0.2000 | 250 | | 3 | 5 | 10 | 15 | 30 | | |
| PWC X2 | 8.385 | 100.00 | 50.00 | 0.2000 | 500 | | 3 | 5 | 10 | 15 | 30 | | |
| PWC Y2 | 8.485 | 100.00 | 50.00 | 0.2000 | 250 | 1500 | 3 | 5 | 10 | 15 | 30 | 60 | 120 |
| DC Forward | | | | Vector Chambers with 5 sense wires per cell | | | | | | | | | |
| | | | | Data in 21 bytes: 5 bits for plane, 2- 2 byte TDC (beg and end) each hit time in 5 sense wires | | | | | | | | | |
| Drift Cham X1 | 8.735 | 100.00 | 50.00 | 2.00 | 25 | | 21 | 20 | 40 | 420 | 840 | | |
| Drift Cham U1 | 8.785 | 100.00 | 50.00 | 2.00 | 25 | | 21 | 20 | 40 | 420 | 840 | | |
| Drift Cham V1 | 8.835 | 100.00 | 50.00 | 2.00 | 25 | | 21 | 20 | 40 | 420 | 840 | | |
| Drift Cham X2 | 8.885 | 100.00 | 50.00 | 2.00 | 25 | | 21 | 20 | 40 | 420 | 840 | | |
| Drift Cham U2 | 8.935 | 100.00 | 50.00 | 2.00 | 25 | | 21 | 20 | 40 | 420 | 840 | | |
| Drift Cham V2 | 8.985 | 100.00 | 50.00 | 2.00 | 25 | | 21 | 20 | 40 | 420 | 840 | | |
| Drift Cham X3 | 9.035 | 100.00 | 50.00 | 2.00 | 25 | | 21 | 20 | 40 | 420 | 840 | | |
| Drift Cham U3 | 9.085 | 100.00 | 50.00 | 2.00 | 25 | | 21 | 20 | 40 | 420 | 840 | | |
| Drift Cham V3 | 9.135 | 100.00 | 50.00 | 2.00 | 25 | | 21 | 20 | 40 | 420 | 840 | | |
| Drift Cham X4 | 9.185 | 100.00 | 50.00 | 2.00 | 25 | 250 | 21 | 20 | 40 | 420 | 840 | 4200 | 8400 |
| PWCs | | | | These chambers are for use with fast processors. We intersperse Forward Drift Chambers | | | | | | | | | |
| | | | | Data is in 3 bytes | | | | | | | | | |
| PWC X3 | 9.535 | 100.00 | 50.00 | 0.2000 | 500 | | 3 | 5 | 10 | 15 | 30 | | |
| PWC Y3 | 9.635 | 100.00 | 50.00 | 0.2000 | 250 | | 3 | 5 | 10 | 15 | 30 | | |
| PWC X4 | 10.135 | 100.00 | 50.00 | 0.2000 | 500 | | 3 | 5 | 10 | 15 | 30 | | |
| PWC Y4 | 10.235 | 100.00 | 50.00 | 0.2000 | 250 | 1500 | 3 | 5 | 10 | 15 | 30 | 60 | 90 |
| RICH | | | | Data in 2 bytes: this is a digital device, no analog information is kept | | | | | | | | | |
| RICH Start | 10.735 | | | | 2800 | 2800 | 2 | 25 | 100 | 50 | 200 | 50 | 200 |
| RICH End | 20.735 | | | | | | | | | | | | |
| TRD | | | | I have assumed 35 cm for each TRD module which includes a radiator plus one chamber | | | | | | | | | |
| | | | | Data is in 3 bytes | | | | | | | | | |
| TRD X1 | 21.235 | 100.00 | 50.00 | 0.2000 | 500 | | 3 | 2 | 5 | 6 | 15 | | |
| TRD Y1 | 21.585 | 100.00 | 50.00 | 0.2000 | 250 | | 3 | 2 | 5 | 6 | 15 | | |
| TRD X2 | 21.935 | 100.00 | 50.00 | 0.2000 | 500 | | 3 | 2 | 5 | 6 | 15 | | |
| TRD Y2 | 22.285 | 100.00 | 50.00 | 0.2000 | 250 | 1500 | 3 | 2 | 5 | 6 | 15 | 24 | 60 |
| Vee Chamber A | | | | These chambers are not backed up with SSDs in beam region | | | | | | | | | |
| | | | | Data is in 2 bytes | | | | | | | | | |
| Vee A X1 | 22.785 | 100.00 | 100.00 | 0.2000 | 500 | | 2 | 4 | 10 | 8 | 20 | | |
| Vee A Y1 | 22.885 | 100.00 | 100.00 | 0.2000 | 500 | | 2 | 4 | 10 | 8 | 20 | | |
| Vee A U1 | 22.985 | 100.00 | 100.00 | 0.2000 | 500 | | 2 | 4 | 10 | 8 | 20 | | |
| Vee A V1 | 23.085 | 100.00 | 100.00 | 0.2000 | 500 | | 2 | 4 | 10 | 8 | 20 | | |

| Detector | Z position | Active Area (full) | | Pitch | Channels | Channels | Bytes/ | Active Channels | | Bytes/Event | | Bytes Sub Total | |
|-------------------------|------------|--------------------|---------|--|----------|-----------|---------|-----------------|-----|-------------|------|-----------------|------|
| | m | X cm | Y cm | cm | | Sub total | Channel | Average | Max | Average | Max | Average | Max |
| Vee A X2 | 23.185 | 100.00 | 100.00 | 0.2000 | 500 | | 2 | 4 | 10 | 8 | 20 | | |
| Vee A Y2 | 23.285 | 100.00 | 100.00 | 0.2000 | 500 | 3000 | 2 | 4 | 10 | 8 | 20 | 48 | 120 |
| Vee Chamber B | | | | These chambers are not backed up with SSDs in beam region | | | | | | | | | |
| | | | | Data is in 2 bytes | | | | | | | | | |
| Vee B X1 | 29.285 | 100.00 | 100.00 | 0.2000 | 500 | | 2 | 4 | 10 | 8 | 20 | | |
| Vee B Y1 | 29.385 | 100.00 | 100.00 | 0.2000 | 500 | | 2 | 4 | 10 | 8 | 20 | | |
| Vee B U1 | 29.485 | 100.00 | 100.00 | 0.2000 | 500 | | 2 | 4 | 10 | 8 | 20 | | |
| Vee B V1 | 29.585 | 100.00 | 100.00 | 0.2000 | 500 | | 2 | 4 | 10 | 8 | 20 | | |
| Vee B X2 | 29.685 | 100.00 | 100.00 | 0.2000 | 500 | | 2 | 4 | 10 | 8 | 20 | | |
| Vee B Y2 | 29.785 | 100.00 | 100.00 | 0.2000 | 500 | 3000 | 2 | 4 | 10 | 8 | 20 | 48 | 120 |
| Vee Chamber C | | | | These chambers are not backed up with SSDs in beam region | | | | | | | | | |
| | | | | Data is in 2 bytes | | | | | | | | | |
| Vee C X1 | 35.785 | 100.00 | 100.00 | 0.2000 | 500 | | 2 | 4 | 10 | 8 | 20 | | |
| Vee C Y1 | 35.885 | 100.00 | 100.00 | 0.2000 | 500 | | 2 | 4 | 10 | 8 | 20 | | |
| Vee C U1 | 35.985 | 100.00 | 100.00 | 0.2000 | 500 | | 2 | 4 | 10 | 8 | 20 | | |
| Vee C V1 | 36.085 | 100.00 | 100.00 | 0.2000 | 500 | | 2 | 4 | 10 | 8 | 20 | | |
| Vee C X2 | 36.185 | 100.00 | 100.00 | 0.2000 | 500 | | 2 | 4 | 10 | 8 | 20 | | |
| Vee C Y2 | 36.285 | 100.00 | 100.00 | 0.2000 | 500 | 3000 | 2 | 4 | 10 | 8 | 20 | 48 | 120 |
| Pb6 Downstream | | | | Data in 4 bytes: 2 bytes for block address, 2 for value | | | | | | | | | |
| Pb6 Upstream | 36.235 | 100.00 | 100.00 | 5.00 | 1750 | 1750 | 4 | 20 | 40 | 80 | 160 | 80 | 160 |
| Start Magnet 3 | 36.735 | 60.96 | 50.8 | Magnet is BM109 opened up to 20 inch gap and 15 kG, Pt-450 MeV/c | | | | | | | | | |
| End Magnet 3 | 38.735 | 60.96 | 50.8 | This gives a vertical acceptance of ± 6.6 mrad, ± 7.9 horizontal. | | | | | | | | | |
| Vee Chamber D | | | | These chambers are not backed up with SSDs in beam region | | | | | | | | | |
| | | | | Data is in 2 bytes | | | | | | | | | |
| Vee D X1 | 39.235 | 100.00 | 100.00 | 0.2000 | 500 | | 2 | 4 | 10 | 8 | 20 | | |
| Vee D Y1 | 39.335 | 100.00 | 100.00 | 0.2000 | 500 | | 2 | 4 | 10 | 8 | 20 | | |
| Vee D U1 | 39.435 | 100.00 | 100.00 | 0.2000 | 500 | | 2 | 4 | 10 | 8 | 20 | | |
| Vee D V1 | 39.535 | 100.00 | 100.00 | 0.2000 | 500 | | 2 | 4 | 10 | 8 | 20 | | |
| Vee D X2 | 39.635 | 100.00 | 100.00 | 0.2000 | 500 | | 2 | 4 | 10 | 8 | 20 | | |
| Vee D Y2 | 39.735 | 100.00 | 100.00 | 0.2000 | 500 | 3000 | 2 | 4 | 10 | 8 | 20 | 48 | 120 |
| LAC | | | | Fastbus ADC readout, 8 bytes, 4 for address, 4 for data | | | | | | | | | |
| | 39.985 | 162.5 | r=162.5 | 0.0500 | 3500 | 3500 | 8 | 125 | 500 | 1000 | 4000 | 1000 | 4000 |
| | 40.442 | | | | | | | | | | | | |
| Neutron Detector | | | | We enumerate the PwC elements but lump together the 50 interleaved scintillators | | | | | | | | | |
| Scintillators | | 76.00 | 76.00 | | 50 | | 3 | 50 | 50 | 150 | 150 | | |
| PwC X1 | 41.985 | 48.00 | 48.00 | 1.0000 | 48 | | 2 | 25 | 50 | 50 | 100 | | |
| PwC Y1 | 42.035 | 48.00 | 48.00 | 1.0000 | 48 | | 2 | 25 | 50 | 50 | 100 | | |
| PwC X2 | 42.085 | 48.00 | 48.00 | 1.0000 | 48 | | 2 | 25 | 50 | 50 | 100 | | |

